

2015

Towards the development of a forensic DNA biosensor

<https://hdl.handle.net/2144/13962>

"Downloaded from OpenBU. Boston University's institutional repository."

BOSTON UNIVERSITY
SCHOOL OF MEDICINE

Thesis

**TOWARDS THE DEVELOPMENT OF A FORENSIC DNA
BIOSENSOR**

by

ARI DARLOW

B.S. State University of New York College at Buffalo, 2013

Submitted in partial fulfillment of the
requirements for the degree of
Master of Science

2015

© 2015 by
Ari Darlow
All rights reserved

Approved by

First Reader

Catherine Grgicak, Ph.D.
Assistant Professor of Biomedical Forensic Sciences

Second Reader

Sabra Botch-Jones, M.S.
Instructor of Biomedical Forensic Sciences

ACKNOWLEDGMENTS

I would like to thank my family for giving me the strength to carry on. I would like to also thank Eric Snyder, John Nord, Tom Tong, Kevin Hu, Kerrigan, Shepard and Adun for their unwavering support in this difficult process.

TOWARDS THE DEVELOPMENT OF A FORENSIC DNA BIOSENSOR

ARI DARLOW

ABSTRACT

In the forensic DNA field, quantitative PCR (qPCR) is commonly used to quantify the amount of deoxyribonucleic acid (DNA) in evidentiary samples. Though sensitive, this method is prone to error. Electrochemistry-based biosensors have been described as a possible alternative to qPCR. To this end, this work aims to develop a biosensor for forensic quantification by chemisorbing oligonucleotides functionalized to methylene blue onto the surface of gold screen-printed electrodes. Prior to this, the surface characteristics of the screen-printed gold electrode are examined through the use of a well-known redox probe $\text{Ru}(\text{NH}_3)_6^{2+/3+}$. Cyclic voltammetry (CV) and Square Wave voltammetry (SWV) were used to measure the current signal. The Randles-Sevcik equation was used to relate the area of the electrode with the current signal.

Surface examinations of the gold screen-printed electrodes suggested these electrodes are suitable for use as a forensic DNA biosensor. Attempts to bind the oligonucleotide to the gold electrode were conducted. Though binding was successful, the resultant SWV signal suggested methods to chemisorb DNA onto gold surfaces require optimization.

TABLE OF CONTENTS

TITLE.....	i
COPYRIGHT PAGE.....	ii
READER APPROVAL PAGE.....	iii
ACKNOWLEDGMENTS	iv
ABSTRACT.....	v
TABLE OF CONTENTS.....	vi
LIST OF TABLES	ix
LIST OF FIGURES	x
LIST OF ABBREVIATIONS.....	xiv
1.0 Introduction.....	1
1.1 Forensic DNA Analysis.....	1
1.2 Biosensor.....	2
1.2.1 Formation of the Biosensor.....	2
1.2.2 Electrodes.....	5
1.2.3 Loading the Oligonucleotides.....	6
1.2.4 Signal Generation.....	7
1.3 Electrochemical Techniques.....	8
1.3.1 Cyclic Voltammetry.....	9
1.3.2 Square Wave Voltammetry.....	13
1.4 Purpose.....	17
1.4.1 Challenges Associated with qPCR.....	17
1.4.1.1 Degraded DNA Samples.....	17
1.4.1.2 Standard Curve Accuracy.....	17

	1.4.2	Creating a Forensic DNA Biosensor.....	18
2.0		Materials and Methods.....	19
	2.1	Materials and Reagents.....	19
	2.2	Instrumentation and Software.....	20
	2.3	Electrodes and Voltammetry Glassware.....	20
	2.4	Analytical Procedure for Gold Electrodes.....	21
	2.4.1	Evaluating Gold SPE performance using hexaammine ruthenium.....	21
	2.4.2	Estimating the Surface Area of Gold Screen Printed Electrodes.....	22
	2.4.2.1	Double-Layer Capacitance Method.....	23
	2.4.2.2	Tafel/Randles-Sevčik Method.....	24
2.5		Developing a Screen Printed Gold Based Biosensor.....	26
2.6		Desorbing the DNA from the Screen Printed Electrode.....	28
3.0		Results and Discussion.....	29
	3.1	Performance of Gold SPE.....	29
	3.1.1	Reusability of Gold SPE.....	29
	3.1.2	Stability of Gold SPE.....	32
	3.1.3	Reproducibility of Gold SPE.....	35
	3.2	Analysis of Surface Area.....	38
	3.2.1	Double-Layer Capacitance.....	38
	3.2.2	Exchange Current Density and Activation Coefficient.....	39
	3.2.3	Real Surface Area.....	42
	3.2.4	Creation of a DNA biosensor.....	46
	3.3	Recommendation for Forensic Biosensors.....	48

4.0	Conclusion.....	49
5.0	Future Research.....	49
	REFERENCES	51
	CURRICULUM VITAE.....	57

LIST OF TABLES

Table	Title	Page
1	Table 1. Data from the tenth cycle of three repetitive CV measurements from five electrode cards: peak potential (V_f) and peak height (i_p).	30
2	Table 2. Data from the SWV of three different sets of measurements from five electrode cards. The data was determined using baselines set by the analyst.	30
3	Table 3. Data from nine cycles of one CV measurement on five electrode cards in 0.0018 M $[\text{Ru}(\text{NH}_3)_6]^{3+/2+}$ in 0.02 M Tris-HCl.	33
4	Table 4. Data from five consecutive SWV measurements from five electrode cards in 0.0018 M $[\text{Ru}(\text{NH}_3)_6]^{3+/2+}$ in 0.02 M Tris-HCl.	34
5	Table 5. Data from cycle ten of CVs from five different electrodes: peak potential (V_f) and peak height (i_p). Data was taken from three separate runs.	36
6	Table 6. Data from the SWV measurements from five sets of measurements from five different electrode cards. The data was determined using baselines set by the analyst.	36
7	Table 7. Capacitance calculated from cyclic voltammograms obtained when the electrodes were immersed in blank buffer. ND = Not detected from a corrupted data file. Capacitance was calculate in μF .	38

LIST OF FIGURES

Figure	Title	Page
1	Figure 1. A representation of a recognition layer of a biosensor where the strand on the left represents the DNA recognition probe (as shown by the straight black line) anchored to the surface of the electrode and the target strand is the complementary target of the probe strand (the black arrow). Based on a schematic drawn by Nakazato et. al. [11]	4
2	Figure 2. Schematic of a gold screen-printed electrode card. 1) the silver reference electrode 2) the gold counter electrode 3) the gold working electrode.	6
3	Figure 3. A triangular waveform, which illustrates a potential sweep rate of 0.04 (in V/s) between two different potentials [31][57].	9
4	Figure 4. A CV of the redox couple, 0.0018 M $[\text{Ru}(\text{NH}_3)_6]^{+3/+2}$ in 0.02 M Tris-HCl. The potentials are measured against an Ag/AgCl reference electrode. Important portions of the curve are the activation control (black solid arrow) and the background current (gray solid arrow).	11
5	Figure 5. A CV in Echem Analyst™. The black lines (accented with the black arrows) represent the baselines that were automatically placed by the software. The I_p is measured from the top of the curve to the baseline.	12
6	Figure 6. An example of a symmetrical square wave pulse waveform. One cycle takes 4 seconds and consists of one positive and negative pulse [57].	14

7	Figure 7. A staircase waveform. The ΔE_s is 1V and each pulse width is 2 seconds [47].	15
8	Figure 8. An example of a square wave voltammogram [47].	15
9	Figure 9. An example of a square wave voltammogram. The baseline is set manually and is represented by the solid black line.	16
10	Figure 10. Mercaptohexanol interacting with the surface of the electrode to stabilize the probe in an upright position.	27
11	Figure 11. A cartoon showing the effect of the hybridization of the target strand to the recognition layer. A) Without the target strand the redox indicator (methylene blue) will interact with the surface of the electrode causing electrons to transfer between the two producing a current. B) After the target is hybridized there is no electron transfer between the redox indicator and the surface thus causing less current to be produced and a decrease in the signal observed [57].	27
12	Figure 12. Cycle ten of three measurements of an electrode in 0.0018 M Ru[(NH ₃) ₆] ^{+3/+2} in 0.02 M Tris-HCl.	30
13	Figure 13. SWV of three measurements of an electrode in 0.0018 M Ru[(NH ₃) ₆] ^{+3/+2} in 0.02 M Tris-HCl.	30
14	Figure 14. Nine CV cycles from one measurement on one electrode in 0.0018 M [Ru(NH ₃) ₆] ^{3+/2+} in 0.02 M Tris-HCl.	34
15	Figure 15. Five SWV measurements from one measurement on one electrode in 0.0018 M [Ru(NH ₃) ₆] ^{3+/2+} in 0.02 M Tris-HCl.	35

16	Figure 16. Cycle ten of CVs from five electrodes in 0.0018 M $[\text{Ru}(\text{NH}_3)_6]^{3+/2+}$ in 0.02 M TrisHCl.	37
17	Figure 17. SWV measurements from five different electrodes in one set of measurements in 0.0018 M $[\text{Ru}(\text{NH}_3)_6]^{3+/2+}$ in 0.02 M TrisHCl.	37
18	Figure 18. A Tafel plot of the cathodic current. The high field area is in the region of positive overpotentials, while the low field area is in the area around $\eta = 0$ V. The dark grey portion indicates the high field region. The black line represents the linear regression performed on the high field region.	39
19	Figure 19. The exchange current densities for the high field and low field analysis. The high field calculations are on the left (the darker grey) for each electrode and the low field calculations are on the right (the lighter grey) for each electrode. The number on the left denotes the specific electrode and the number on the right denotes the run.	40
20	Figure 20. Graph of the activation coefficients from the high field Tafel analysis of the cathodic curve of 0.0018 M $\text{Ru}(\text{NH}_3)_6^{3+/2+}$. Regarding the electrode used, the number to the left of the decimal point denotes the specific electrode used and the number to the right denotes the run.	41
21	Figure 21. Surface area calculations of the gold working electrode using the C_{dl} model in the blank buffer.	42
22	Figure 22. Surface area calculations of the gold working electrode using the quasi-reversible Randles-Sevcik method in $\text{Ru}(\text{NH}_3)_6^{3+/2+}$.	43
23	Figure 23. The comparison of both of the calculation methods for real surface area.	44
24	Figure 24. A SWV of the bare gold layer (dark grey) and the MCH layer (light grey).	47

25	Figure 25. A SWV of the bare gold layer (dark grey), the DNA layer (the arrow pointing to the data) and the MCH layer (light grey).	48
----	---	----

LIST OF ABBREVIATIONS

A	amperes
bp	base pairs
©	copyright
CV	cyclic voltammetry/voltammogram
DC	direct current
DNA	deoxyribonucleic acid
dsDNA	double-stranded DNA
e-	electron
F	farad
PBS	phosphate buffered saline
PCR	polymerase chain reaction
qPCR	quantitative polymerase chain reaction
®	registered trademark
R ²	coefficient of determination
RSD	relative standard deviation
SE	standard error
SPE	screen-printed electrodes
ssDNA	single-stranded DNA
STR	short tandem repeat
TCEP	tris(2-carboxyethyl)phosphine

TM	trade mark
V	volt
VNTR	variable number of tandem repeats

1.0 Introduction

Human identification and forensic DNA, or deoxyribonucleic acid, analysis utilize various methods designed to detect DNA at low quantities. These methods tend to be robust and have low limits of detection; some are even able to detect DNA from a single cell. Forensic DNA methods typically utilize the polymerase chain reaction, or PCR, to detect low quantities of DNA. Despite the low limit of detection associated with PCR-based chemistries, optimal results are usually garnered when the input target mass is approximately 0.5 ng. Because an optimal mass is targeted, there is a need for a quantification method that will provide robust, accurate quantification such that optimized DNA processes may be chosen.

1.1 Forensic DNA Analysis

The practice of forensic DNA analysis started in the 1980s with an article published in *Nature* by Jeffreys et al. This article described a method that could differentiate segments of the DNA sequence that are highly variable between individuals. These locations were named minisatellites and contained variable numbers of tandem repeats (VNTRs) ^[1]. These minisatellite regions contain approximately 10 to 1000 repeating units, with each unit containing 10 to 100 base pairs. Due to the size of VNTR loci, the DNA has to be of excellent quality and a large number of copies must be present in order to successfully identify the source of a biological stain ^{[2][3]}.

In contrast, STR or short tandem repeat (STR) analysis, which uses PCR, solves some of the issues related to VNTR analysis. PCR was first described in a

Science article by Mullis et al. which used PCR analysis to help diagnose Sickle Cell Anemia [4]. This method takes segments of DNA and replicates them at an exponential rate if the reaction proceeds efficiently. Current forensic practice dictates that human identity testing incorporates the amplification of STRs, which are two to six base pair units repeated approximately 4 to 50 times [2][5]. This technique is used currently in forensic DNA labs due to the lower limit of detection, high sensitivity and high power of discrimination [3].

1.2 Biosensor

Due to the error associated with qPCR and quantifying DNA, modified electrodes have been proposed as a means to quantify DNA cheaply and efficiently [44]. Biosensors are electrodes that are modified with a biochemical molecule, which targets a specific analyte in a sample. The interaction between the analyte and the biological molecules at the electrode surface produce an electrochemical signal, which is directly related to the properties of the sample. Biosensors are currently used in other fields including anti-body detection and other molecular diagnostic fields [29][64-65]. This project focuses on developing a screen-printed gold biosensor as an alternative to the current qPCR technique used in forensic laboratories. In order to accomplish this, a detailed understanding of the underlying gold surface is necessary. Thus, a full characterization of the gold electrode is warranted.

1.2.1 Formation of the Biosensor

Biosensors are typically created using a solid electrode surface and electrostatically or chemically tethering biological molecules to the surface.

Electrostatic adsorption of DNA is achieved by applying a positive potential to the electrode, which attracts the negatively-charged DNA molecule. Chemisorption may be used to produce a biological layer and is achieved by chemically binding a modified probe to the surface of the electrode. Chemically modified surfaces are typically one molecule thick and are specific to a target in the solution that is undergoing experimentation. This layer is termed 'recognition layer' due to this specificity. Electrochemical signals are produced when the biosensor is placed into a sample containing the analyte. These signals are characteristic to the analyte in question and can be used to detect the quantity of the sample of interest [7].

The use of human sequence-specific oligonucleotides that target particular genomic sequences creates a DNA biosensor. The oligonucleotides are complementary to a sequence on the target molecule and are approximately 18-40 base pairs long [8]. This oligonucleotide is typically engineered to identify a DNA sequence that is highly conserved so that the experiment can be reproduced. If this particular sequence occurs once in a single copy of the DNA, the absolute number of the molecules present can be more easily quantified. Forensic DNA analysis already uses oligonucleotides suitable for this type of analysis. This study makes use of primers that target a region of TPOX [10].

An example of one type of DNA biosensor is shown in Figure 1. An oligonucleotide is tethered to the surface of the electrode and if the targeted DNA molecule is in solution, the hybridization affinity of complementary DNA strands causes the complementary strand to hybridize to the short DNA molecule attached

to the surface of the electrode. It should be noted that one target DNA molecule is assumed to bind to one recognition layer molecule [7]. After hybridization occurs, the electrochemical signal obtained from the target DNA molecules can be measured in order to estimate how much DNA is present in solution.

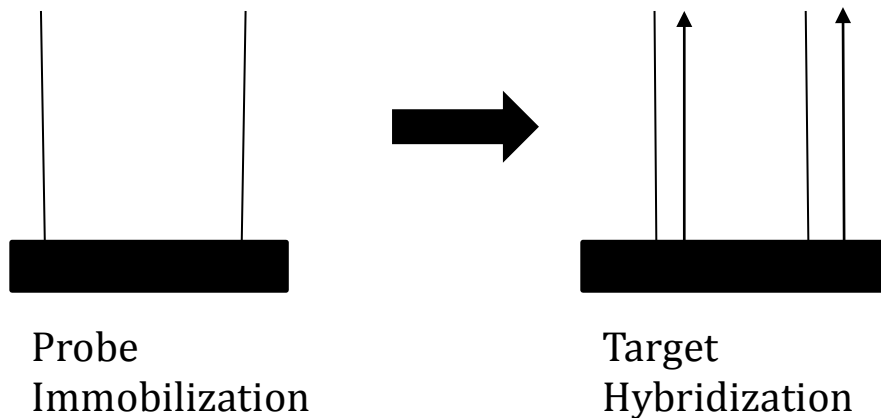


Figure 1. A representation of a recognition layer of a biosensor where the strand on the left represents the DNA recognition probe (as shown by the straight black line) anchored to the surface of the electrode and the target strand is the complementary target of the probe strand (the black arrow). Based on a schematic drawn by Nakazato et. al. [11]

This assay is expected to have a dynamic range which is dependent upon a number of factors. First, the range of concentration that the biosensor is able to detect will be influenced by the loading capacity of the probe onto the surface of the electrode [12]. Thus, surface area of the electrode, steric hindrances, and the fractional surface coverage will all impact the dynamic range [14-15] [59]. Further, the range is hypothesized to be dependent on the hybridization efficiency of the target to the recognition layer. Also, the sample will not be quantified accurately if the DNA strands re-anneal to the original complementary strand before the measurement takes place. Urea and Formamide can denature the DNA strands, but it has been

shown that these chemicals could interfere with the annealing of the probe to the target ^{[16][17]}.

1.2.2 Electrodes

Carbon and gold have arisen as the materials of choice for this type of work ^[18]. These materials are used mainly in solid disk form, which are expensive and bulky. Newer electrodes come as a thick-film screen-printed patterned electrode ^{[8][19]}. Gold has been extensively investigated as an electrode foundation for these types of reactions because of its relative inertness, its favorable electron transfer kinetics, and its large anodic potential range.

Thick-film screen-printed patterned electrodes have also been researched as small, low cost, disposable options for biosensor development ^[8] and are commercially available ^{[13][18]}. Typically, metals are deposited on a plastic or ceramic card as an ink mixture. The electrode and the leads that connect the electrical contacts to the electrode are all printed as ink on the substrate. A non-conduction layer is then placed on the card, which defines the exposed electrode areas. A typical ink mixture consists of particles mixed with a binder/adhesive, and a solvent. The binder aids in the adhesion of the ink to the card while the solvent is used to maintain a desired viscosity of the ink mixture.

These screen-printed electrode cards are typically produced as a three-electrode system which includes the working, reference, and counter electrodes. Thus, these electrodes are laid out in a planar array. For the electrode card used in this study, the reference electrode is situated between the working and counter

electrode. The counter electrode is larger than the working electrode and wraps around the electrode as shown in Figure 2. During an electrochemical experiment, the potential is applied to the working electrode with respect to the reference electrode. The current that is generated as a result of the applied potential is passed between the counter and working electrodes.

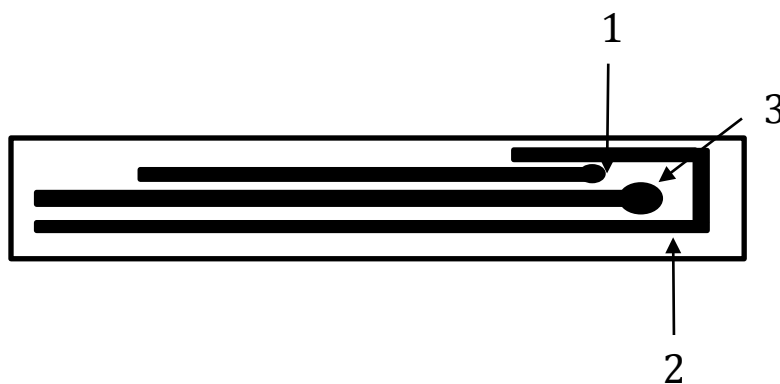


Figure 2. Schematic of a gold screen-printed electrode card. 1) the silver reference electrode 2) the gold counter electrode 3) the gold working electrode.

The reference electrode in this case is silver/silver chloride and is printed on the card in silver ink [24]. The electrode is stabilized by chloride ions in the solution and all samples that are run using the electrode ought to contain a chloride ion source for the applied potential of this system to be reliable [22].

As appealing as screen-printed electrodes can be, there are some downfalls associated with their use. Previous studies have shown that there is a substantial level of chlorine on the surface of the electrode, presumably from the binder used to produce the ink. Thus, despite cleaning the electrode by cycling from large positive

to large negative potentials for several cycles in sulfuric acid, chlorine may still remain on the surface [13][19][49].

1.2.3 Loading the Oligonucleotides

Several studies have generated a recognition layer and characterized the effects different molecules have on the electrode. For example, Herne and Tarlov showed that by using thiol-derivatized single-stranded DNA, a recognition layer can be created through covalent bonding of the sulfur atom and through non-specific interactions of the DNA with the surface of the electrode [17]. For most applications, in order to create the recognition layer of the biosensor using gold electrodes and chemisorption, chemical interactions between the probe and the surface must occur. To accomplish this the probe is modified at one end with a thiol group; the thiol covalently bonds to the electrode surface through the formation of a sulfur-gold bond, creating the recognition layer. In this experiment, a mixed monolayer was created using the DNA probe and mercaptohexanol (MCH), an alkanethiol with a terminal hydroxyl group. The MCH is used to prevent non-specific adsorption of DNA to the surface of the electrode and controls the formation of the recognition layer. Levicky et al. explored the use of MCH and the formation of the recognition layer [66]. Through the use of neutron reflectivity, the distance of the DNA from the gold surface was measured before and after exposure to MCH. It was observed that after the DNA was exposed to MCH, the thickness profile of the chemisorbed DNA increased, suggesting that the DNA was lifted off the surface due to the formation of the MCH layer. These data suggest that with MCH the DNA that forms the

recognition layer would remain in an upright position with only one contact point to the surface. This orientation allows for efficient hybridization of the target DNA.

1.2.4 Signal Generation

To generate an electrochemical signal, several probes have been studied. Some quantitation methods use direct signal. For example, the use of the current produced from the oxidation of guanine residues present in a DNA sample can be used to quantify the amount of DNA on the surface of the electrode. Alternatively, measuring the capacitance of an electrochemical system when the target hybridizes to the recognition layer can also be used [8][25-28]. Another method of detection is the addition of an indicator molecule to the electrolyte. This could take the form of an electrostatic or intercalating molecule, which is used as the redox probe.

Electrostatic indicators work by electrostatically interacting with the DNA. In contrast, intercalating compounds 'insert' themselves in between the bases of double-stranded DNA [7]. Examples of intercalators include ethidium bromide and methylene blue. Examples of electrostatic probes include $\text{Ru}(\text{NH}_3)_6^{2+/3+}$ or $\text{Fe}(\text{CN}_6)^{3-}/4-$. Another method involves functionalizing the DNA probe with an indicator molecule; due to the single-stranded DNA's flexibility, the indicator molecule can interact with the surface of the electrode, soliciting high signal response. After hybridization with the target strand, the DNA on the recognition layer becomes double-stranded and therefore rigid, which causes a decrease in the observed signal due to the indicator's inability to interact with the surface [29].

1.3 Electrochemical Techniques

Common electrochemical techniques to detect electron transfer reactions can be used to characterize the electrode, recognition layer, and hybridized sample.

Potentiodynamic techniques that evaluate the current and potential (or voltage) in an electrochemical cell, and the relationship between the two, can be used for this purpose [30]. Below are descriptions of two voltammetric techniques used during this study: cyclic voltammetry and square wave voltammetry.

1.3.1 Cyclic Voltammetry (CV)

Cyclic voltammetry is a technique that utilizes direct current (DC), where the potential is swept between two values at a constant scan rate and the current is measured during these runs. These potential values are chosen so that the potential at which the analyte is expected to reduce/oxidize is within the potential scan range.

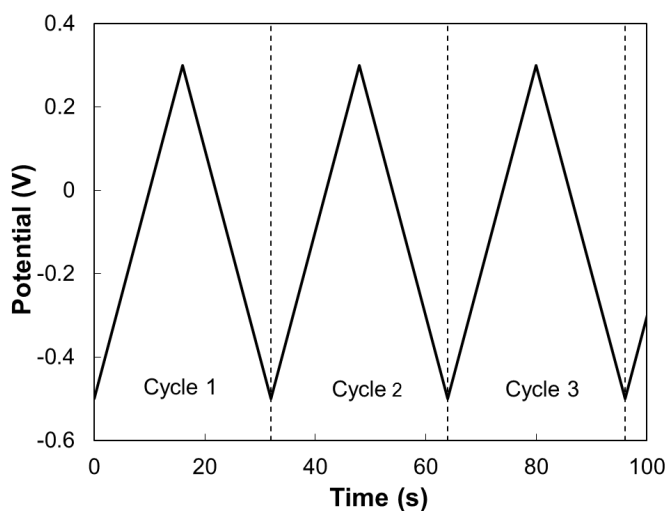
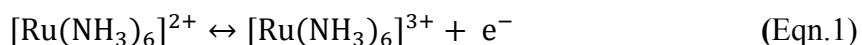


Figure 3. A triangular waveform, which illustrates a potential sweep rate of 0.04 (in V/s) between two different potentials^{[31][57]}.

Figure 3 illustrates the relationship between potential and time during a CV experiment^[32]. For this study, the analyte of interest chosen to characterize the gold surface was the reversible redox probe hexaammine ruthenium, $\text{Ru}(\text{NH}_3)_6^{3+/2+}$. Each cyclic voltammogram is run at 10 cycles that overlay over each other. By using a reversible redox couple, a steady-state voltammogram can be obtained. There are two different potential sweeps: a positive and a negative sweep. The more positive potentials represent the oxidation of the analyte, which is described by:



This is representative of the anodic sweep. The reverse of this reaction occurs during the cathodic sweep, which elicits the reduction of the ruthenium hexaammine as the potential of the working electrode becomes more negative^[33]. The current data can be presented as current density, which is the current value typically normalized to the nominal surface area of the electrode. There are a number of properties of the voltammogram used during analysis. There is a background current, known as a charging current^[34]. This charging current is subtracted from the peak signal during common CV analysis if the scan ranges are sufficiently large enough in order to allow the peaks to fully develop; signals derived from activation controlled processes can also be evaluated. In the activation controlled region, there is an exponential increase in current, due to the conversion of reactants to products at the surface of the electrode. This is the result of direct electron transfer from the analyte and is called faradaic current. The current will

eventually reach a maximum and then tail off due to mass transport, or diffusion, control limitations [22][35].

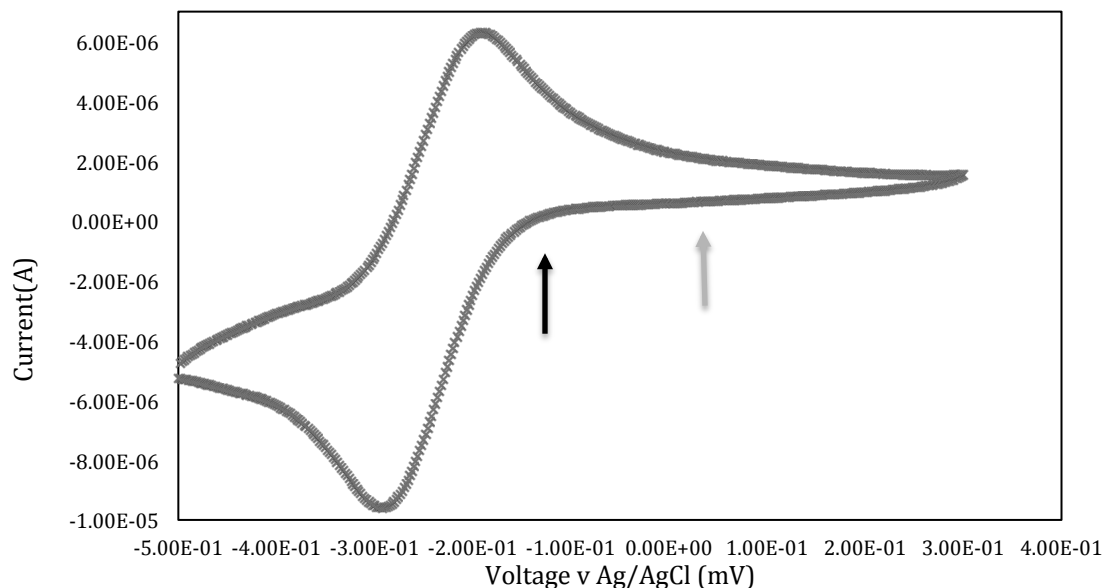


Figure 4. A CV of the redox couple, 0.0018 M $[\text{Ru}(\text{NH}_3)_6]^{+3/+2}$ in 0.02 M Tris-HCl. The potentials are measured against an Ag/AgCl reference electrode. Important portions of the curve are the activation control (black solid arrow), and the background current (gray solid arrow).

Figure 4 is an example of a typical CV graph. The axes are set as the current on the y-axis and the potential on the x-axis. The parameters of interest are extracted from the CV. The relationship between signal and potential at various regions of the graph provide a plethora of information. For example, V_f , or peak potential and i_p , or the peak height, can provide information regarding whether the reaction is electrochemically reversible.

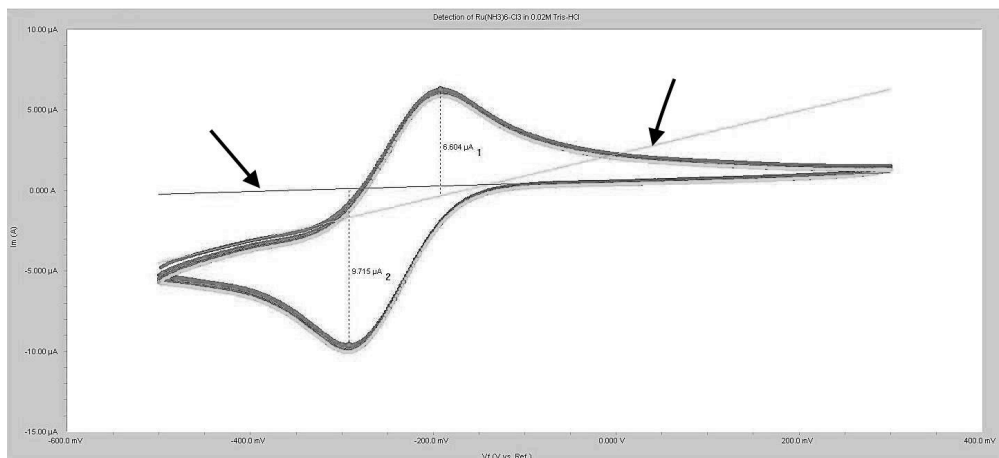


Figure 5. A CV in Echem Analyst™. The black lines (accented with the black arrows) represent the baselines that were automatically placed by the software. The i_p is measured from the top of the curve to the baseline.

Figure 5 demonstrates the method by which the charging current is subtracted from the total signal to obtain i_p . Subsequently, i_p can be used to determine a number of items, such as the concentration of the analyte by using the reversible Randles-Sevcik equation:

$$i_p = 0.4463 nFAC \left(\frac{nFvD}{RT} \right)^{1/2} \quad (\text{Eqn. 2})$$

where i_p is the peak current (in A), n is the number of electrons transferred in a half reaction, A is the surface area of the electrode (in cm^2), C is the concentration of the analyte (in mol/cm^3), v is the scan rate (in V/s), D is the diffusion coefficient of the analyte (in cm^2/s), R is the universal gas constant (in $\text{J}/\text{mol}^*\text{K}$), and T is the temperature (in K) [33]. Alternatively, the modified Randles-Sevcik equation can be used in instances where the reaction is electrochemically quasi-reversible:

$$i_p = (2.99 \times 10^5) n(\alpha n)^{1/2} AC(D)^{1/2}(v)^{1/2} \quad (\text{Eqn. 3})$$

This equation incorporates the activation coefficient, α , into the equation. This coefficient is a parameter which is related to the energy barrier of the system. The activation coefficient can be determined through evaluating the relationship between current and potential. A value of 0.5 is commonly used as an approximation; however, an empirically determined value of α is utilized in this study^[22]. Overpotential is defined as:

$$\eta = E_{cell} - E^o \quad (\text{Eqn. 4})$$

where η is the overpotential (in V), and E^o (in V) is the equilibrium potential of the system. Overpotential is a measure of deviation from electrochemical equilibrium^{[22][37]}. At large values of overpotential, the Tafel equation (shown in Eqn. 8) can be used to solve for the exchange current density (i_o) and the activation coefficient (α). The Tafel range, which is based on a high-field approximation of the Butler-Volmer relationship, is reached at 52 mV of overpotential at room temperature when α is 0.5^{[22][37]}.

1.3.2 Square Wave Voltammetry (SWV)

Square wave voltammetry (SWV) is a derivative of pulse voltammetry. Pulse voltammetry measures the current that is produced following the application of a potential pulse as a function of time^[30]. It has been shown that this technique produces fast and sensitive results providing detection limits down to a concentration of 10^{-8} M^[38].

Square wave voltammetry is a combination of a staircase waveform and a symmetrical square wave pulse^[39]. The symmetrical square wave pulse is defined

as a potential that is applied almost instantaneously for a fixed period of time. This is also identified as the positive pulse. The negative pulse is defined as the period of time after the potential returns to the initial potential and holds there for a pulse width. One cycle of a SWV consists of a positive and negative pulse [40]. Amplitude is defined as the change in voltage between the initial voltage and the pulse voltage.

This potential waveform is depicted in the following figure:

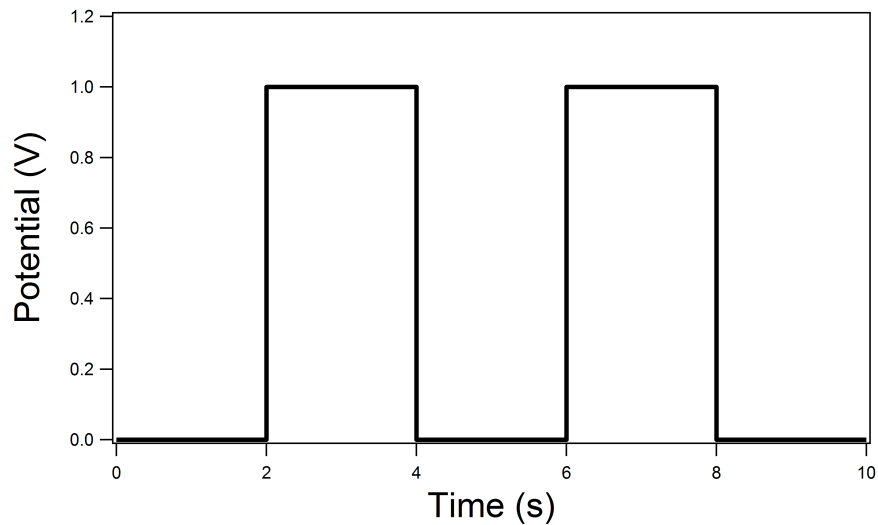


Figure 6. An example of a symmetrical square wave pulse waveform. One cycle takes 4 seconds and consists of one positive and negative pulse [57].

The staircase waveform consists of a constant pulse width and an increasing potential. The change in potential or ΔE_s is constant for each potential increase [30].

This staircase waveform is depicted in this next figure:

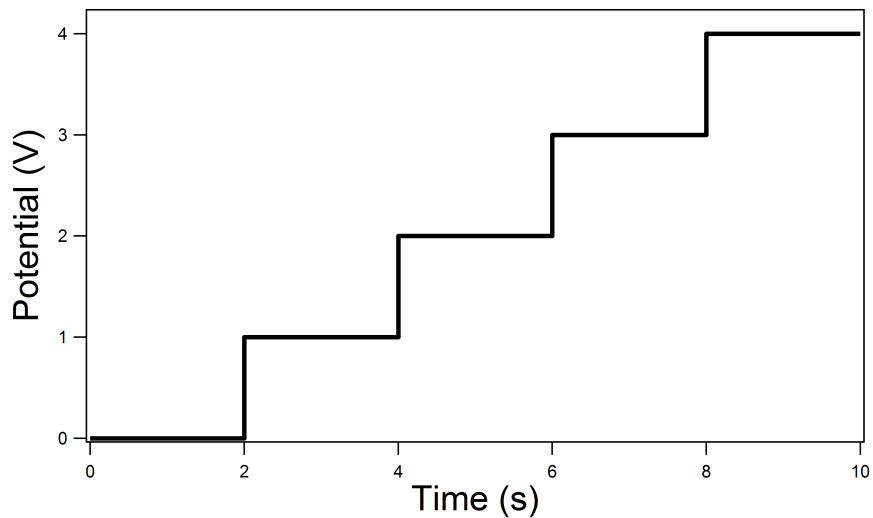


Figure 7. A staircase waveform. The ΔE_s is 1V and each pulse width is 2 seconds [47].

When these two waveforms are combined, this results in a square wave voltammetry waveform.

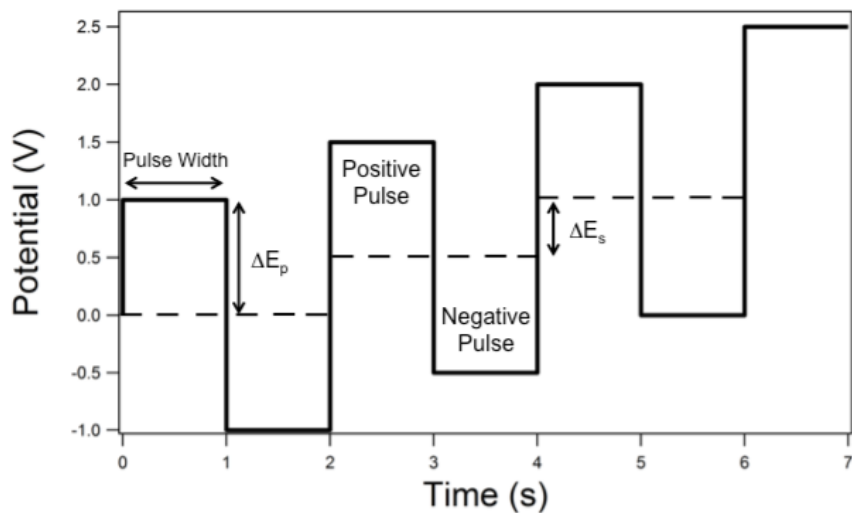


Figure 8. An example of a square wave voltammogram [47].

The parameters that were described in the individual waveforms are utilized in the above figure. Change in potential, or ΔE_p is analogous to the symmetrical

square wave pulse's amplitude. The net current (i_{net}) of this waveform is determined as such:

$$i_{net} = i_{positive} - i_{negative} \quad (\text{Eqn. 5})$$

where $i_{positive}$ is the current measured from the positive pulse while $i_{negative}$ is the current from the negative pulse [38]. When the net current is plotted against potential, the graph appears as a peak. To analyze this peak, a linear baseline is set and the height of the peak is measured from the apex of the peak to the baseline. Peak height can also be correlated to the concentration of analyte in the sample [30].

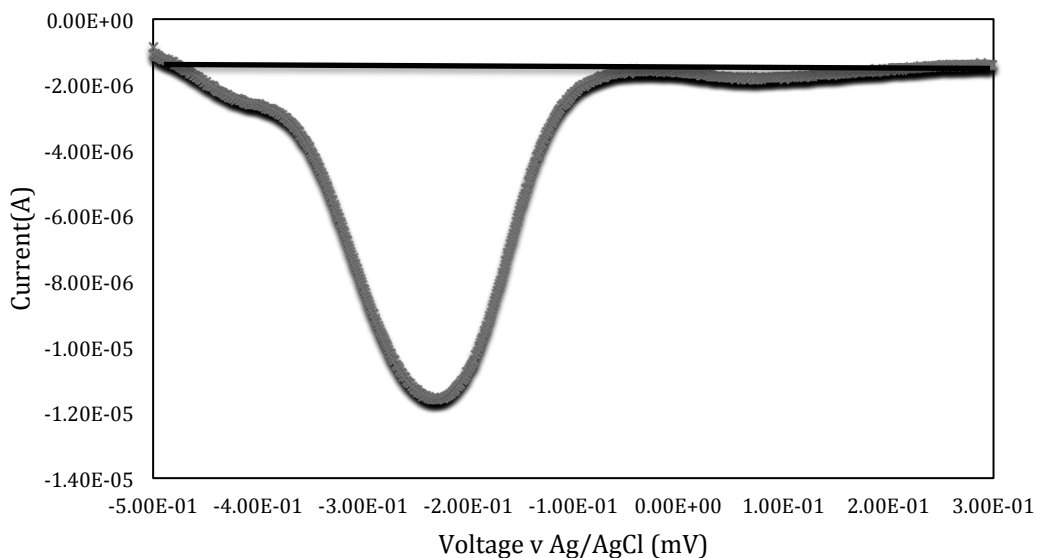


Figure 9. An example of a square wave voltammogram. The baseline is set manually and is represented by the solid black line.

1.4 Purpose

The purpose of this research was to develop a biosensor, using gold screen-printed electrodes, to offer a robust technique that could potentially replace quantitative PCR. Given the following problems associated with qPCR, biosensors could introduce an assay that will quantify forensic samples faster and cheaper than methods currently used.

1.4.1 Challenges Associated with qPCR

1.4.1.1 Degraded DNA Samples

In order for qPCR to function properly, the sequence that is to be amplified has to be present in a single, continuous strand or else the primers will not anneal properly. A sample of DNA that is degraded will be fractured in certain areas and in this case the amplification will not proceed. If the sample is severely degraded the calculated concentration will misrepresent the actual amount of DNA present. Timken et al. showed that for severely degraded samples the amplification could fail and it will appear that the questioned sample contains no DNA ^[41].

1.4.1.2 Standard Curve Accuracy

The creation of a standard curve is used to accurately quantify unknown forensic samples. Absolute qPCR quantification requires a set of serial dilutions that create samples of known concentrations in order to determine unknown quantities of DNA from evidence.

The challenges with producing an accurate standard curve have been well documented, and even manufacturers will explicitly state that the quality of the

pipettes used and discrepancies in the concentrations can affect accuracy [9].

Further, Smith and Osborn showed that significant errors in the initial quantification of the standard sample caused sample-to-sample variation [43]. This research was supported by Grgicak et al. who found that there was significant variability introduced due to pipetting errors and suggested quantities of DNA can be determined using a single calibrator [44].

1.4.2 Creating a Forensic DNA Biosensor

Taking into consideration the aforementioned issues associated with qPCR, it is of interest to create a biosensor that will offer a robust analytical procedure for the quantification of DNA in forensic samples. This can also lead to the development of an assay that can simultaneously quantify the DNA and assess the extent of the degradation in the sample. Thus, the purpose of this research is to analyze the ability to load single-stranded DNA which will recognize a complementary strand of DNA and generate a signal that correlates to the amount of DNA in the sample onto the surface of gold screen-printed electrodes. These electrodes and recognition layers were tested for their reproducibility and repeatability by measuring the change in current density using a quasi-reversible redox couple and assessing any changes in the active surface area of the electrode.

As shown by Wang, electrochemical techniques are possible alternatives to PCR based methods because they are as sensitive [45], and as specific as PCR based systems, as shown by Keraan et al., and do not require potentially costly machines [7]. Recent research has shown that biosensors can be used in other applications,

such as clinical diagnostics, food and environmental testing and DNA analysis^{[27][46]}.

It is this project's goal to extend the application of biosensors into the field of forensic DNA analysis.

2.0 Materials and Methods

2.1 Materials and Reagents

The chemicals used were prepared with materials purchased from Sigma Aldrich (St. Louis, MO) and Fisher Scientific (Waltham, MA) unless stated otherwise. Deionized water (DI) of 18.2 M Ω ·cm resistivity was used to make all solutions. The solutions used in the experiment were as follows: hexamine ruthenium (III) chloride; 10 mM tris(2-carboxyethyl)phosphine (TCEP); 0.5 M sulfuric acid H₂SO₄; 0.01 M potassium chloride (KCl)/0.1 M H₂SO₄; alumina slurry; a phosphate buffered saline solution (PBS) at pH 7.4; 2mM mercaptohexanol (MCH); and 0.5 M potassium hydroxide (KOH). The hexaammine ruthenium (III) chloride was purchased from Sigma Aldrich. Hexaammine ruthenium (III) chloride was prepared in a 0.02 M Tris-HCl buffer solution to a final concentration of 0.0018 M. The PBS pH 7.4 buffer was prepared by combining 2.92 g of sodium chloride with 0.069 g sodium phosphate monobasic, 0.071 g sodium phosphate dibasic, 50 mL of 1 M magnesium chloride and 25 mL of deionized water. The pH was then adjusted to 7.0-7.2 with concentrated sodium hydroxide and then brought to a final volume of 50 mL.

The ssDNA probe used was ordered from Biosearch Technologies, Inc. (Novato, CA). The probe was modified with methylene blue at the 3' end of the strand and a thiol C6 linker at the 5' end. The strand sequence was as follows:

5'-Thiol C6 SS-CGGGAAGGGAACAGGACTAAG- Methylene Blue- 3'

A 200 μM stock solution was prepared in PBS pH 7.4.

2.2 Instrumentation and Software

The voltammetric measurements were performed on a Series GTM 750 Potentiostat/Galvanostat/ZRA instrument in tandem with FrameworkTM, version 6.11 and Echem AnalystTM, version 6.11 software (Gamry Instruments, Warminster, PA). Data was exported from the Echem Analyst interface to Microsoft Excel [®] for additional analysis.

2.3 Electrodes and Voltammetry Glassware

Screen-printed gold electrodes (SPE) were purchased from the Pine Instrument Company (Grove City, PA). Each electrode consisted of a working electrode, a gold counter electrode and a silver/silver chloride reference electrode. The electrodes are screen-printed on ceramic substrates and the traces, which connect the electrode to the edge-card type connector, are insulated with a chemically resistant layer of ceramic ^[18]. The edge card connector holds the electrode in place and a mini-B USB connects the electrode to the potentiostat.

There were two types of glassware that were purchased from Pine Instrument Company for this experiment. The first was a glass vial that holds approximately 20 mL of liquid. This was used primarily for cleaning procedures and some analytical procedures. The second glass vial has a Teflon insert at the bottom, which has a slit-like void in the center that holds approximately 1 mL of liquid. The second vial was used during the runs which used $\text{Ru}(\text{NH}_3)_6^{2+/3+}$ as the redox probe.

2.4 Analytical Procedure for Gold Electrodes

2.4.1 Evaluating Gold SPE performance using hexaammine ruthenium

The performance and stability of the gold screen-printed electrodes were measured using cyclic voltammetry and a reversible redox probe, hexaammine ruthenium ($[\text{Ru}(\text{NH}_3)_6]^{3+/2+}$). Hexaammine ruthenium was at a concentration of 0.0018 M in 0.02 M Tris-HCl buffer pH 7.2. Five screen-printed electrodes were purchased from Pine Instrument Company and used to measure reproducibility, stability and repeatability. Reusability was assessed by the evaluation of i_p and V_f between five identical CV measurements performed on one electrode. Stability was evaluated by assessing the deviation in i_p and V_f between 10 CV cycles in one run. Reproducibility was measured by assessing the same parameters between similar CV measurements performed on the five electrodes.

The working electrode was cleaned with 0.05 μM alumina. The alumina was lightly applied in a circular motion with a gloved finger for three minutes. After rinsing the alumina slurry off the surfaces, the electrode card was sonicated for five minutes. The electrodes were then electrochemically cleaned. To do this, electrodes were placed in 0.5 M sulfuric acid and set at +2 volts for 5 seconds and -0.35 V for 10 seconds. Cleaning of the electrode surfaces continued by scanning over a potential of -0.35 to +1.5 V 20 times at a rate of 4 Vs^{-1} . Further, four additional cycles which ranged from -0.35 to 1.5 V at a rate of 0.1 Vs^{-1} were performed. The electrodes were then submerged in 0.01 M KCl/0.1 M sulfuric acid and a CV was performed for 10 scans at a rate of 0.1 Vs^{-1} , over four potential ranges: +0.2 to +0.75

V, +0.2 to +1.0 V, +0.2 to +1.25 V and +0.2 to +1.5V. This process was performed to remove any organic contaminants that may have been left on the surface of the electrodes from the printing procedure [14]. Once the electrodes were cleaned, a blank measurement of the bare gold electrode was taken using CV and SWV techniques. The 'blank signal' was obtained while the card was immersed in 0.02 M Tris-HCl buffer by using the following electrochemical parameters: 1) CV- a potential range of -0.5 to 0.3 V with a scan rate of 0.05 V/s at 10 cycles and a max current of 0.05 mA; 2) SWV- a potential range of -0.4 to 0.3 V with a pulse size of 25 mV, a step size of 1 mV and a max current of 0.1 mA. After the blank measurement was taken, the electrodes were placed in the ruthenium solution and the same run parameters were utilized to obtain the signal.

The data were examined in Echem Analyst™ to evaluate the: peak potential (V_f , in mV) and height of the peak (i_p , in μA). The peak height was calculated in relation to a baseline that was extrapolated from a part of the data that came before the peak. These parameters were compared to ascertain the reproducibility, stability and reusability of the five electrodes. The averages, standard deviations and percent relative standard deviations (RSD) were calculated for each parameter and compared.

2.4.2 Estimating the Surface Area of Gold Screen Printed Electrodes

The nominal surface area of the working electrodes is known. However, this value is not equal to the real electrochemical surface area. The surface of screen-printed electrodes is not pristine [14], which may affect the active surface area of the

electrode. Further, changes in the real surface area may occur during activation or if the electrode is pretreated as shown in studies conducted by Churinsky, Su and Wang [14][48][49]. This study estimated the active surface area of the working gold electrode using two different methods of calculation, both of which are described below.

2.4.2.1 Double-Layer Capacitance Method

When a potential is applied to a working electrode in a blank buffer, a charging current is observed [34]. Therefore, an estimate of the capacitance can be calculated from CV's using the following equation:

$$C_{dl} = \frac{I_a - I_c}{2v} \quad (\text{Eqn. 6})$$

where C_{dl} is the double layer capacitance (in Faraday units, F), I_a is the anodic current (in amperes, A), I_c is the cathodic current (in amperes, A) and v is the scan rate of the experiment (0.05 V/s) [50]. This equation was used under the assumption that the electrode was behaving as a parallel plate capacitor and that the source of the resistance originated from the solution [50].

After the double layer capacitance was estimated, the surface area of the working electrode was calculated using the following [34]:

$$A = \frac{C_{dl}l}{\epsilon\epsilon_0} \quad (\text{Eqn. 7})$$

where A is the active surface area of the working electrode (in m²), l is the separation of the plates in a double-layer capacitor (3 X 10⁻¹⁰ m) [34], C_{dl} is the capacitance value calculated above, ϵ_0 is the permittivity of free space (8.854 X 10⁻¹²

F/m) and ϵ is the dielectric constant for the solution ($\epsilon= 11$ was used for this work) [51].

2.4.2.2 Tafel/Randles-Sevčik Method

The Tafel slope and Randles-Sevčik equation were utilized to calculate the active surface area of the gold electrode, which is derived from the electron transfer with a redox couple such as hexaammine ruthenium (III) chloride. To perform the Tafel analysis, the data were transformed from potential (V) and current (A) to overpotential (η , in V) and the natural logarithm of current density ($\ln(i)$, A/cm²), respectively. The overpotential was calculated as per Equation 4.

Tafel analysis is typically used to determine two values: the exchange current density (i_o) and the activation coefficient (α). The cathodic sweep curve was used for analysis and the activation coefficient obtained through Tafel analysis was used in the quasi-reversible Randles-Sevčik equation (Eqn. 3) to determine the active surface area of the working electrode. The peak height of the cathodic curve was also used.

Tafel analysis utilizes the linear region of the natural logarithm of current versus overpotential curve. A linear regression analysis, starting at approximately 52 mV was applied. The following equation describes the Tafel relationship:

$$\ln(i) = \ln(i_o) + \frac{\alpha F}{RT} \eta \quad (\text{Eqn.8})$$

where i is the current density (in A/cm²), i_o is the exchange current density (A/cm²), α is the activation coefficient, F is the Faraday constant (9.64×10^4 C/mol), R is the universal gas constant (8.314 J/mol*K), T is the temperature (298.15 K) and η is the

overpotential (V). It is noted that the Tafel equation (Eqn. 8) is derived from the Butler-Volmer equation during high field analysis. Thus, the resultant slope obtained by ordinary least squares linear regression can yield the activation coefficient.

Once the activation coefficient was calculated, the modified Randles-Sevčik equation (Eqn. 3) was rearranged and applied to calculate the active surface area [54]:

$$A = \frac{i_p}{(2.99 \times 10^5)n(\alpha n)^{1/2}C(D)^{1/2}(v)^{1/2}} \quad (\text{Eqn. 9})$$

where A is the active surface area (cm^2), i_p is the peak height of the cathodic current relative to the baseline set (A), n is the number of electrons transferred during the reaction (1 electron is transferred), α is the activation coefficient, C is the concentration of the analyte ($1.8 \times 10^{-6} \text{ mol/cm}^3$), D is the diffusion coefficient of ruthenium ions in solution ($8.8 \times 10^{-6} \text{ cm}^2/\text{s}$) [55] and v is the scan rate (0.05 V/s).

The low field approximation of the Butler-Volmer equation was also used in order to calculate the exchange current density using the following equation and a linear regression analysis. In this analysis the data were plotted as overpotential (V) versus current density (A/cm^2):

$$i = i_o \frac{nF}{RT} \eta \quad (\text{Eqn. 10})$$

This low field analysis is only applicable to small overpotentials, typically $\pm 5 \text{ mV}$ about OCV [25].

2.5 Developing a Screen Printed Gold Based Biosensor

The procedure for the creation of this biosensor was previously described by Rowe et al. [29]. To generate the biosensor, 1 μL of 200 μM single stranded DNA probe was added to 2 μL of 10 mM of tris(2-carboxyethyl) phosphine (TCEP) and incubated for 1 hour in the dark at room temperature. A second 2 μL aliquot of TCEP was added and the mixture was incubated in the dark for one hour at room temperature. TCEP is mainly used for its reduction properties in order to break S-S bonds of the thiol group. The probe was diluted to a concentration of 200 nM with 995 μL of PBS at pH 7.5. The electrodes were cleansed by utilizing the same process outlined in section 2.4.1.

A blank was taken by using SWV, with a potential range of 0.0 to -0.6 V, a pulse size of 25 mV, and a step size of 1 mV, a frequency of 50 Hz and a max current of 0.1 mA. The electrode was then submerged in 200 nM DNA probe solution and incubated for one hour to allow the DNA to chemisorb to the gold surface through the formation of gold-sulfur covalent bonds between the gold surface and the reduced thiol on the probe. The DNA modified electrode was then submerged in 2 mM mercaptohexanol for 1 hour. Mercaptohexanol was used in this process because it has been shown to aid in the prevention of the non-covalent bonding between the DNA and the electrode surface. This stabilizes the tethered DNA such that it remains in an upright position as depicted in Figure 10 [56].

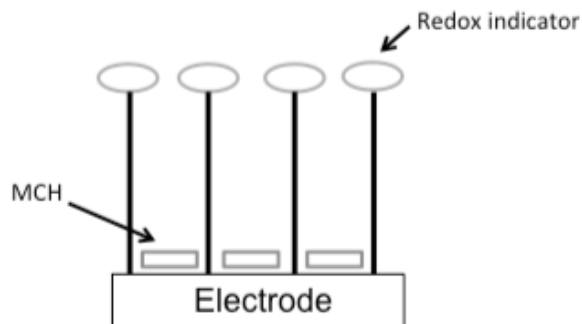


Figure 10. Mercaptohexanol interacting with the surface of the electrode to stabilize the probe in an upright position.

After the incubation period, the electrode was rinsed for one minute with DI water, to remove any excess mercaptohexanol from the electrodes. The electrode was then submerged in PBS (pH 7.4) in the electrochemical cell for ten minutes. SWV was performed. The SWV was run from 0.0 to -0.6 V, a pulse size of 25 mV, a step size of 1 mV, a frequency of 50 Hz and a max current of 0.1 mA. The peak was expected to appear around -0.35 V, based on the known redox potential associated with methylene blue [29].



Figure 11. A schematic showing the effect of the hybridization of the target strand to the recognition layer. A) Without the target strand the redox indicator (methylene blue) will interact with the surface of the electrode causing electrons to transfer between the two producing a current. B) After the target is hybridized there is no electron transfer between the redox indicator and the surface thus causing less current to be produced and a decrease in the signal observed [57].

All analyses were performed using Echem Analyst v. 6.11. A linear baseline was set using the *linear fit* function, and the peak height was measured against the baseline.

2.6 Desorbing the DNA from the Screen Printed Electrode

In order to reuse gold electrodes, the DNA had to be desorbed from the surface. This was accomplished by immersing the biosensor in 0.5 M KOH and linearly sweeping the potential 25 times from -0.25 to -1.3 V. Peaks in the data appeared at approximately -1020 mV, indicating the desorption of mercaptohexanol and at -560 mV, indicating the desorption of the DNA probe. When the number of runs increased, the strength of the peaks decreased, signifying that the DNA molecules were desorbing from the surface of the electrode [58]. One LSV was run per adsorption of recognition layer.

3.0 Results and Discussion

3.1 Performance of Gold SPE

Cyclic Voltammograms from each electrode card in the ruthenium hexaammine experiment were examined in multiple parts. The 10th cycle of five consecutive measurements on a single card was examined to determine reusability. The signal from 10 consecutive cycles within a CV run was then examined to assess stability, and the signal from the tenth cycle between measurements of five different electrodes was then examined to determine reproducibility. This analysis was

completed for both CV and SWV to determine if both electrochemical analysis methods are reusable, stable and reproducible.

The parameters that were estimated from the SWV were the peak potential (V_f) and peak current (i_p) from baseline as described in Section 1.3.1.

3.1.1 Reusability of Gold SPE

First, each electrode was used five times in succession to determine reusability of each electrode card. The variation between the measurements of potential (V_f) and the peak height (i_p) were determined. Qualitatively, it was observed that the CVs vary to a large extent due to the increase in baseline. However, the potential as well as i_p remained stable throughout the experiment. The variation in i_p , observed via % relative standard deviation (RSD) ranged from 1.5% to 17.5% in cathodic peak height. The peak height obtained during the anodic sweep resulted in an RSD range of 2.4% to 13%. Further, SWV also resulted in little variation in the measurements with RSD values of peak currents of less than 16%. Similarly the V_f RSDs are in the same range of those obtained from the i_p 's. Figure 12 and 13 show the raw data obtained when three CV and SWV runs recorded from one electrode card, respectively.

Table 1. Data from the tenth cycle of three repetitive CV measurements from five electrode cards: peak potential (V_f) and peak height (i_p).

		Anodic			Cathodic		
		Average	Stdev	RSD(%)	Average	Stdev	RSD(%)
$i_p(\mu\text{A})$	E1	6.4	0.2	3.6	-9.9	0.1	1.5
	E2	6.3	0.2	2.4	-11.9	2.1	17.5
	E3	6.4	0.4	5.9	-9.7	0.8	8.3
	E4	6.7	0.6	8.2	-10.1	0.7	6.5
	E5	6.4	0.8	13.0	-10.0	0.8	7.9
$V_f(\text{mV})$	E1	-187.9	2.0	1.1	-299.3	6.1	2.0
	E2	-181.9	6.0	3.3	-302.0	14.0	4.6
	E3	-189.9	2.0	1.0	-300.6	6.5	2.2
	E4	-184.0	2.0	1.1	-300.6	4.9	1.6
	E5	-186.7	1.2	0.6	-302.6	11.4	3.8

Table 2. Data from the SWV of three different sets of measurements from five electrode cards. The data was determined using baselines set by the analyst.

	$i_p(\mu\text{A})$			$V_f(\text{mV})$		
	Average	Stdev	RSD(%)	Average	Stdev	RSD(%)
E1	-9.1	0.9	10.1	-233.0	4.5	1.9
E2	-8.4	0.9	10.2	-229.8	6.1	2.7
E3	-9.7	0.6	6.5	-230.0	1.8	0.8
E4	-8.0	1.0	12.9	-226.2	3.5	1.5
E5	-8.5	1.3	15.5	-226.5	4.0	1.8

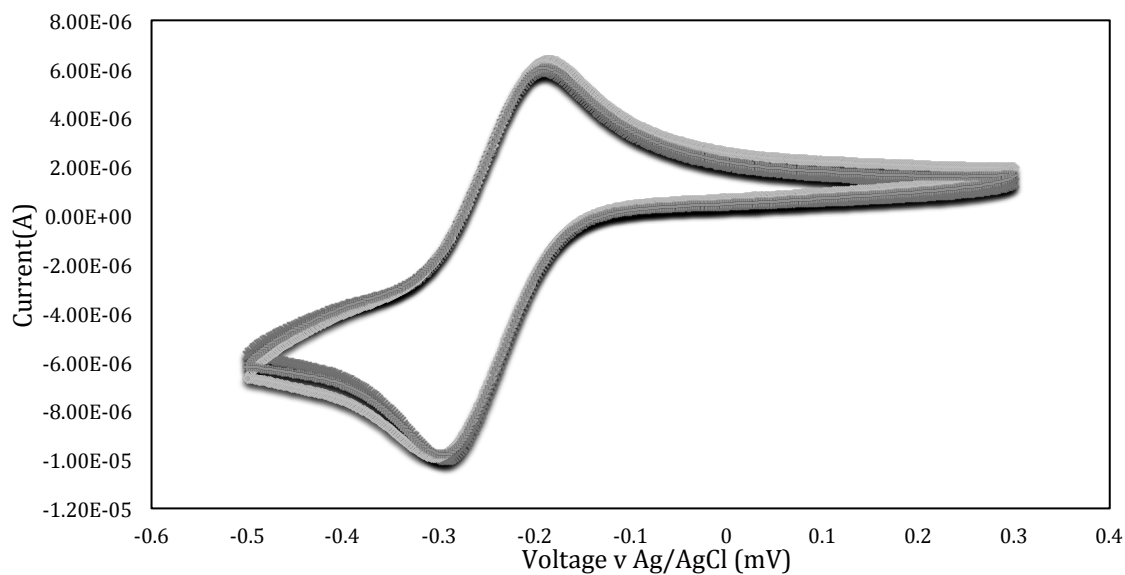


Figure 12. Cycle ten of three CV runs of a single electrode card in 0.0018 M $\text{Ru}[(\text{NH}_3)_6]^{+3/+2}$ in 0.02 M Tris-HCl.

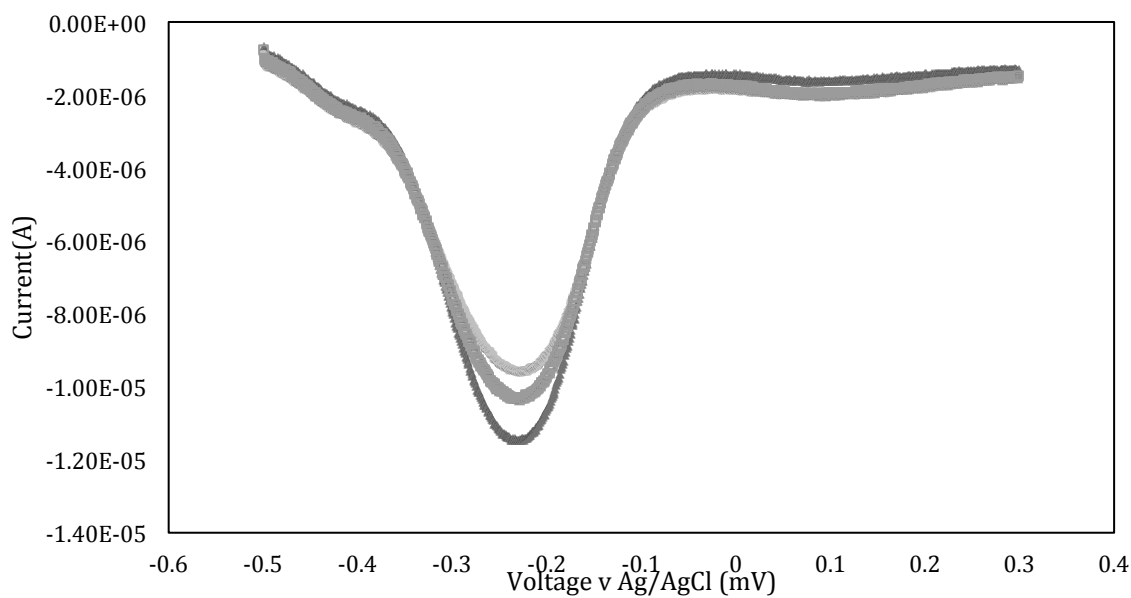


Figure 13. SWV of three runs of a single electrode card in 0.0018 M $\text{Ru}[(\text{NH}_3)_6]^{+3/+2}$ in 0.02 M Tris-HCl.

3.1.2 Stability of Gold SPE

Each cycle of a CV from each of the five electrodes was compared to determine stability of the electrode card. To measure stability, the electrochemical system passes through several cycles and if the voltammograms are similar between cycles the system may be considered stable. This system may be classified as stable when the curves are similar in shape and the V_f and i_p are consistent. Since the first CV is rarely similar to subsequent cycles, the first cycle was not used in this analysis. A summary of the results of 10 cycles for each of the five electrode cards is provided in Table 3. This summary includes the average, standard deviation, and relative standard deviation (RSD). The voltage applied during the experiment is controlled, in part, by the reference electrode; by examining these potential values, it can therefore be determined if the entire system, including the reference electrode, is stable [22]. These data show there is little variation in the V_f , which signifies that the reference electrode, electrolyte concentrations, and working electrode surfaces were stable over the period of time in which measurement was taken. This has also been observed by Vanysek et al. on screen-printed carbon electrode cards, who showed that potential values did not deviate from a 20 mV range [21].

Further, the current stability was determined by the peak height (i_p) of each cycle. The average, standard deviation, and RSD for these data are reported in Table 3. Little variation was detected in the V_f and i_p measurements, which suggested that the gold working electrode, the silver counter electrode, and the reference electrode were stable. Furthermore, data from the anodic sweeps varied more than the data

taken from the cathodic sweeps. The CV measurements showed a larger variation in the i_p measurement, with RSD values up to 18.1%, but the V_f measurement showed little variation, with RSD values of less than 6%. SWV showed similar results. These data indicated overall stability of the cell. Figure 14 and 15 show the CV and SWV obtained for cycles two through 10 on one representative card, respectively.

Table 3. Data from nine cycles of one CV measurement on five electrode cards in 0.0018 M $[\text{Ru}(\text{NH}_3)_6]^{3+/2+}$ in 0.02 M Tris-HCl.

		Anodic			Cathodic		
		Average	Stdev	RSD(%)	Average	Stdev	RSD(%)
$i_p(\mu\text{A})$	E1	6.7	0.3	4.4	-9.9	0.2	1.5
	E2	6.4	1.0	15.5	-14.0	0.3	1.9
	E3	6.8	0.3	4.8	-9.9	0.1	1.1
	E4	7.3	0.3	4.6	-9.3	1.7	18.1
	E5	7.3	0.3	3.6	-10.8	0.2	1.8
$V_f(\text{mV})$	E1	-191	1.0	-0.5	-292.6	1.3	0.5
	E2	-178	1.8	-1.0	-313.7	3.2	1.0
	E3	-191	1.0	-0.5	-289.1	17.3	6.0
	E4	-181	1.0	-0.6	-299.1	1.0	0.3
	E5	-188	0.9	-0.5	-289.9	0.9	0.3

Table 4. Data from five consecutive SWV measurements from five electrode cards in 0.0018 M $[\text{Ru}(\text{NH}_3)_6]^{3+/2+}$ in 0.02 M Tris-HCl.

	$i_p(\mu\text{A})$			$V_f(\text{mV})$		
	Average	Stdev	RSD(%)	Average	Stdev	RSD(%)
E1	-8.9	0.4	4.3	-234	4	1.9
E2	-7.9	0.1	1.1	-231	8.0	3.4
E3	-10.1	0.1	0.8	-229.3	0.6	0.2
E4	-7.9	0.1	1.2	-227	3.0	1.3
E5	-7.6	0.1	0.7	-225	4	1.7

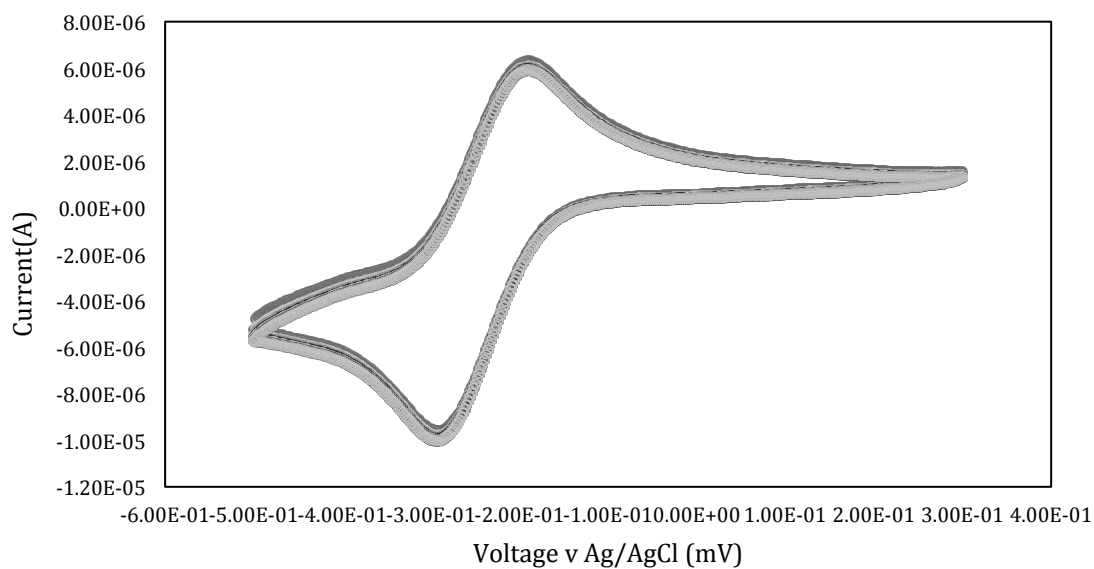


Figure 14. Nine CV cycles from one measurement on one electrode in 0.0018 M $[\text{Ru}(\text{NH}_3)_6]^{3+/2+}$ in 0.02 M Tris-HCl.

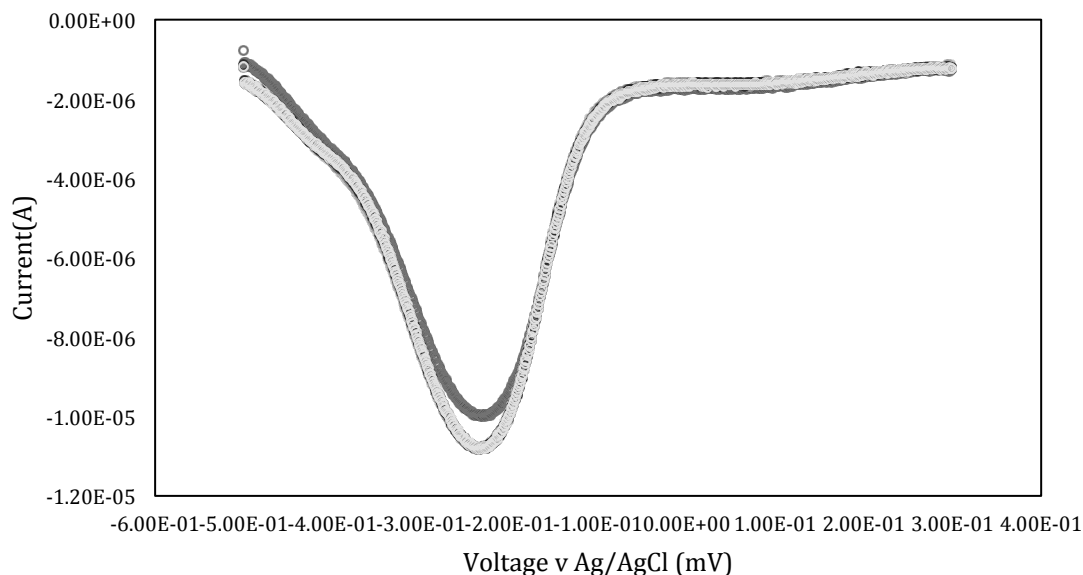


Figure 15. Five SWV measurements from one measurement on one electrode in 0.0018 M $[\text{Ru}(\text{NH}_3)_6]^{3+/2+}$ in 0.02 M Tris-HCl.

3.1.2 Reproducibility of Gold SPE

The tenth cycle of a CV measurement from five electrodes was compared to determine the reproducibility of the system. The average, standard deviation, and RSD were calculated as well. The RSD of the parameters were low, which is confirmed qualitatively by the CVs, and resulted in almost identical curves. The variation in anodic and cathodic i_p over the five electrode cards was as high as 6.3% and 16.9% (Table 5), respectively. Similarly, the RSD between runs of one electrode was as high as 13% and 17.5% (Table 1) for the anodic and cathodic i_p , respectively. This signifies that the variation between electrode cards is similar to the variation obtained within a card, suggesting any validation or quality control systems would not necessarily be required to take inter-card reproducibility into account. The SWV showed similar results whereby the i_p measurement resulted in RSD values as high

as 20.8% (Table 6). These values are similar to the maximum RSD of 15.5% for the i_p values obtained during reusability tests (Table 2). Since the variation in signal between cards is similar to the variation obtained within one card, development of biosensors is expected to be a function of the efficiency of adsorption or other factors, rather than changes in the gold surface structure between cards.

Table 5. Data from cycle ten of CVs from five different electrodes: peak potential (V_f) and peak height (i_p). Data was taken from three separate runs.

		Anodic			Cathodic		
		Average	Stdev	RSD(%)	Average	Stdev	RSD(%)
$i_p(\mu A)$	Run 1	6.8	0.4	6.3	-11.0	1.9	16.9
	Run 2	6.3	0.4	5.9	-10.2	0.4	3.6
	Run 3	6.2	0.3	4.4	-10	1.0	10.4
$V_f(mV)$	Run 1	-186	7	3.5	-230	10	3.4
	Run 2	-186	2	1.2	-307	4	1.2
	Run 3	-187	2	1.2	-297	6	2.2

Table 6. Data from the SWV measurements from five sets of measurements from five different electrode cards. The data was determined using baselines set by the analyst.

	$i_p(\mu A)$			$V_f(mV)$		
	Average	Stdev	RSD(%)	Average	Stdev	RSD(%)
Run 1	-9.3	0.7	7.3	-229	3	1.4
Run 2	-9	2	20.8	-229	8	3.3
Run 3	-10	1.0	10.0	-229.5	0.5	0.2
Run 4	-8.2	0.5	5.6	-229	3	1.2
Run 5	-8	1	14.2	-226	4	1.9

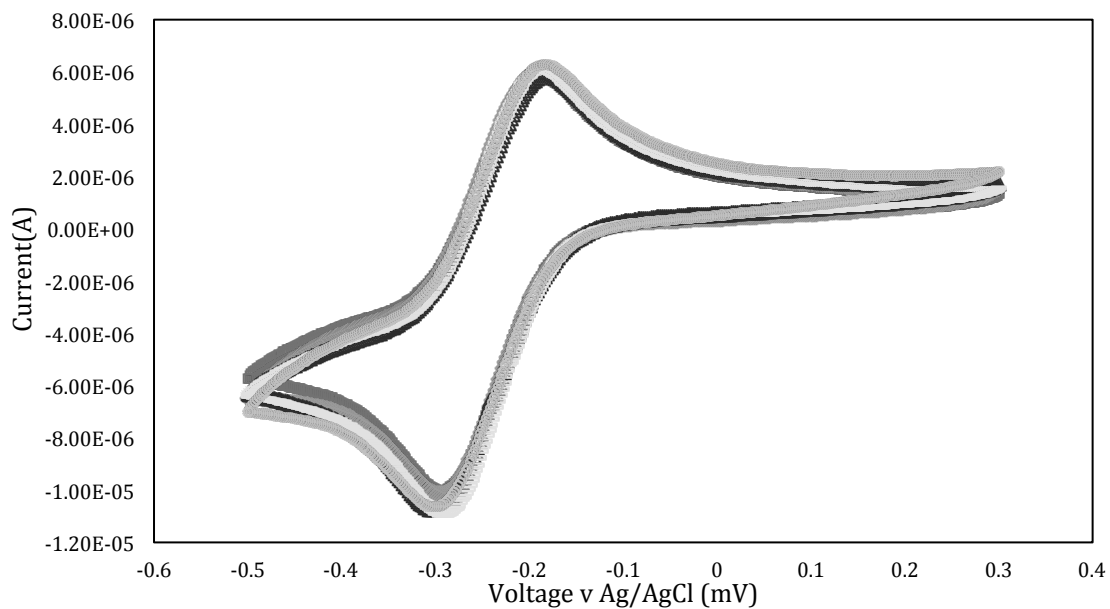


Figure 16. Cycle ten of CVs from five electrodes in 0.0018 M $[\text{Ru}(\text{NH}_3)_6]^{3+/2+}$ in 0.02 M TrisHCl.

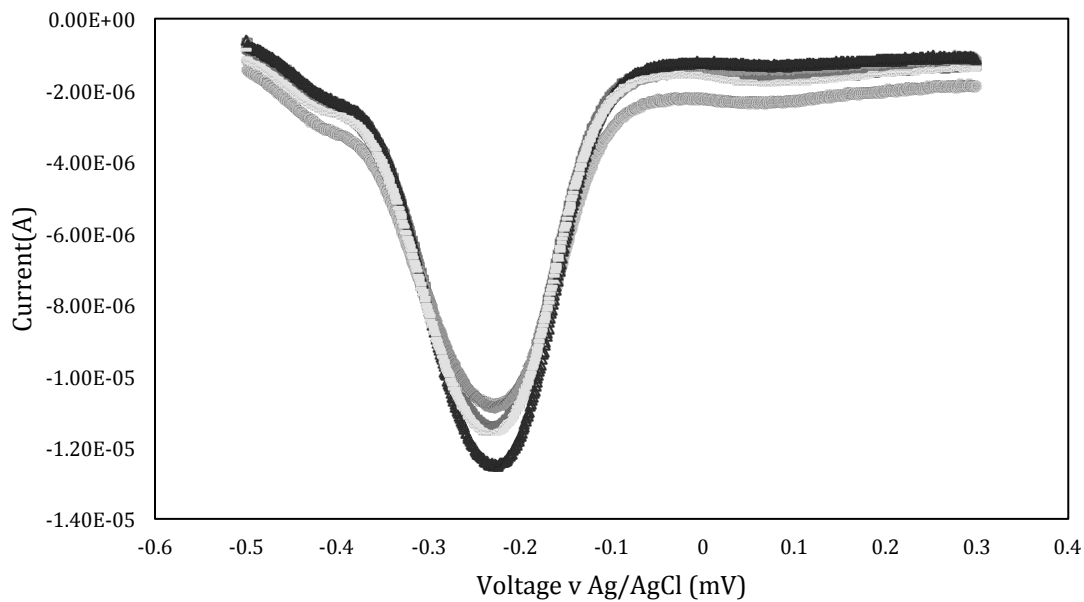


Figure 17. SWV measurements from five different electrodes in one set of measurements in 0.0018 M $[\text{Ru}(\text{NH}_3)_6]^{3+/2+}$ in 0.02 M TrisHCl.

3.2 Analysis of the Surface Area

The next study used charging current in blank buffer and peak current in the ruthenium hexaammine solution to approximate the active surface area of the screen-printed electrodes.

3.2.1 Double-Layer Capacitance

The measurements in the blank buffer were performed with the same five gold SPEs. Each electrode was immersed in blank buffer and a CV was run three times. This totaled fifteen measurements. The cathodic and anodic sweeps were analyzed to determine double-layer capacitance, C_{dl} , between the Tris-HCl buffer and the working electrode surface. The results are shown below.

Table 7. Capacitance calculated from cyclic voltammograms obtained when the electrodes were immersed in blank buffer. ND = Not detected from a corrupted data file. Capacitance was calculate in μF .

	E1	E2	E3	E4	E5
Run 1	1.8	5.2	2.8	4.3	3.5
Run2	1.8	2.5	2.8	1.3	1.8
Run3	2.2	3.8	5	3.3	5.3
Run4	3.5	5.3	6.8	1.7	5.2
Run5	ND	1.6	1.5	3.3	3.6
Average	2.3	3.7	3.8	2.8	3.9
STD	0.8	1.6	2.1	1.2	1.5
RSD(%)	34.0	44.4	55.8	44.9	37.8

3.2.2 Exchange Current Density and Activation Coefficient

The experiment using ruthenium hexaammine with these electrodes consisted of three runs on each of the five electrodes.

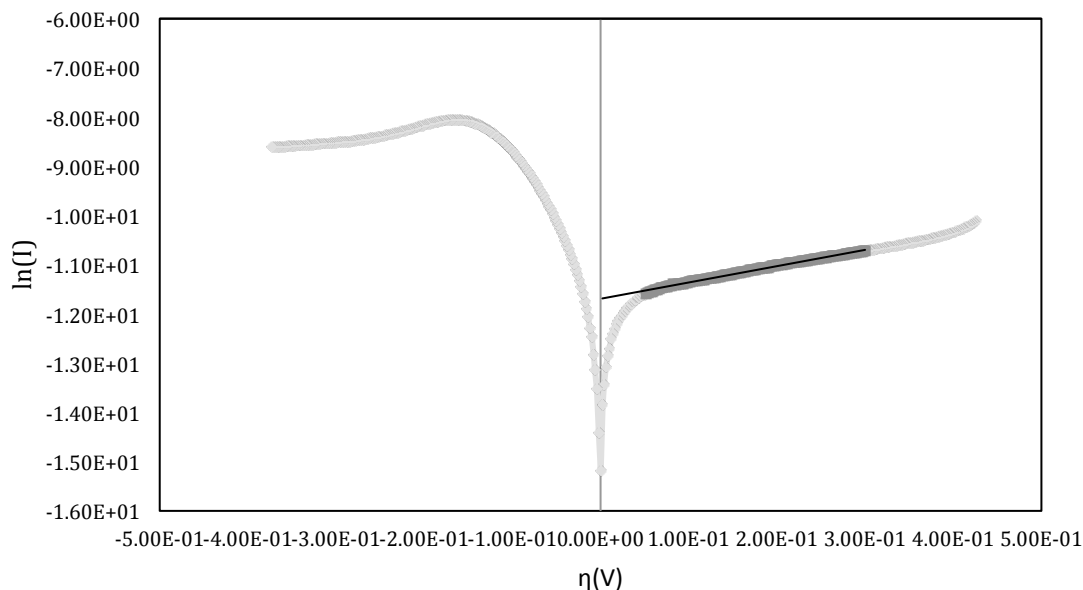


Figure 18. A Tafel plot of the cathodic current. The high field area is in the region of positive overpotentials, while the low field area is in the area around $\eta = 0$ V. The dark grey portion indicates the high field region. The black line represents the linear regression performed on the high field region.

A Tafel slope analysis was performed on each of these CV runs to determine the exchange current density (i_0) and the activation coefficient (α). All of the data was suitable for linear regression analysis. A high field analysis and low field analysis were conducted on each set of the data providing 15 results for the high field analysis and 15 low field analysis results.

The exchange current density is a measure of the reaction rate of the system when it is at equilibrium. It cannot be directly measured as it describes the kinetics of the electrochemical system at OCV (open circuit voltage), which means there is no

net reaction. However, i_0 can be determined using either ^[22] the high and low field regions of a natural log (current) versus overpotential (η) curve. The high field method examines a section of system whereby the overpotential is greater than 52 mV.

The low field method examines a section of the curve that is approximately ± 5 mV from $\eta = 0$ mV. In this region the relationship between the current density and overpotential is linear and by using an ordinary least squares regression the parameters of interest can be determined and evaluated. The following graph shows the exchange current density values calculated from the linear regression analysis (the dark and light grey bars).

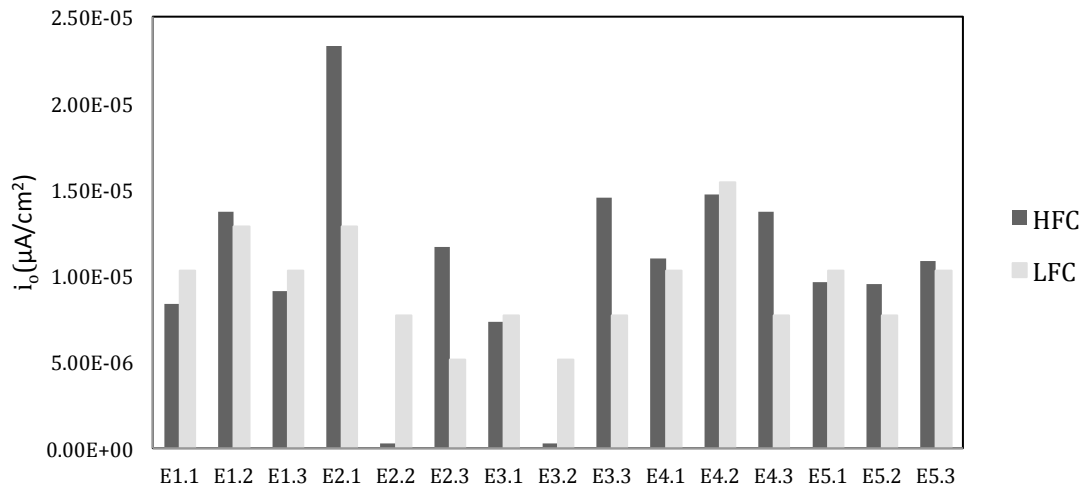


Figure 19. The exchange current densities for the high field and low field analysis. The high field calculations are on the left (the darker grey) for each electrode and the low field calculations are on the right (the lighter grey) for each electrode. The number on the left denotes the specific electrode and the number on the right denotes the run.

The graph above shows that, in general, the exchange current density values for both high field and low field are similar. A paired t-test was also conducted on the sets of data to determine if the high field and low field calculations were

significantly different from one another. For all of the exchange current values the t_{stat} number is lower than the t_{critical} number, which means that the two sets of data are not significantly different from one another.

The next value calculated was the activation coefficient (α). The α is related to the energy of activation of the electrochemical system. This can also be calculated using the high field method.

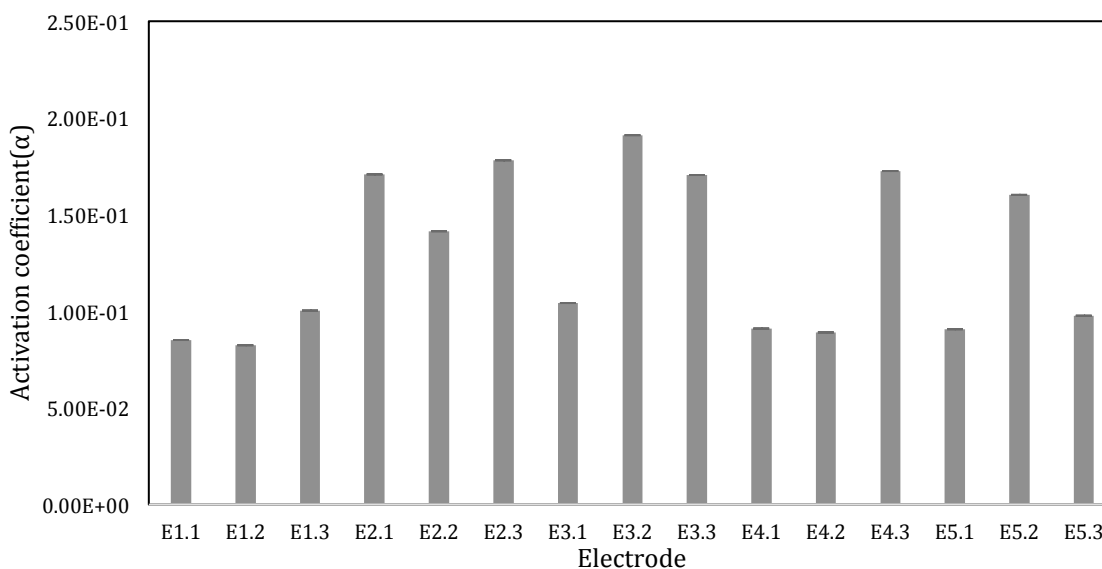


Figure 20. Graph of the activation coefficients from the high field Tafel analysis of the cathodic curve of 0.0018 M $\text{Ru}(\text{NH}_3)_6$. Regarding the electrode used, the number to the left of the decimal point denotes the specific electrode used and the number to the right denotes the run.

As observed above, the activation coefficient is not the same across all of the electrodes and runs. The activation coefficients are less than 0.5 which is the expected value for the activation coefficient for simple, single electron transfer at room temperature [22].

3.2.3 Real Surface Area

After i_o , α and C_{dl} were calculated, the real surface area of the working gold electrode was calculated using two methods: 1) the quasi-reversible Randles-Sevcik method as per Equations 8 and 9 and 2) the double layer capacitance method as detailed in Equations 6 and 7. For the quasi-reversible Randles-Sevcik the activation coefficient used was the experimentally determined values (Figure 20). The next graphs represent the active surface areas calculated via the double-layer capacitance method (Figure 21) and the quasi-reversible Randles-Sevcik (Figure 22).

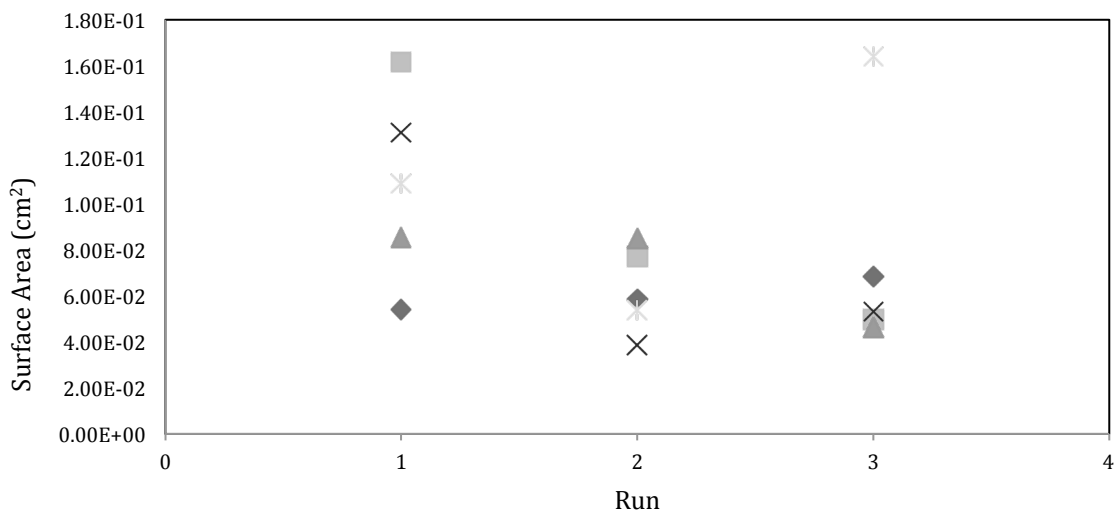


Figure 21. Surface area calculations of the gold working electrode using the C_{dl} model in the blank buffer. Electrode 1 are the diamonds, Electrode 2 are the squares, Electrode 3 are the triangles, Electrode 4 are the x's and Electrode 5 are the x's with a line running through them.

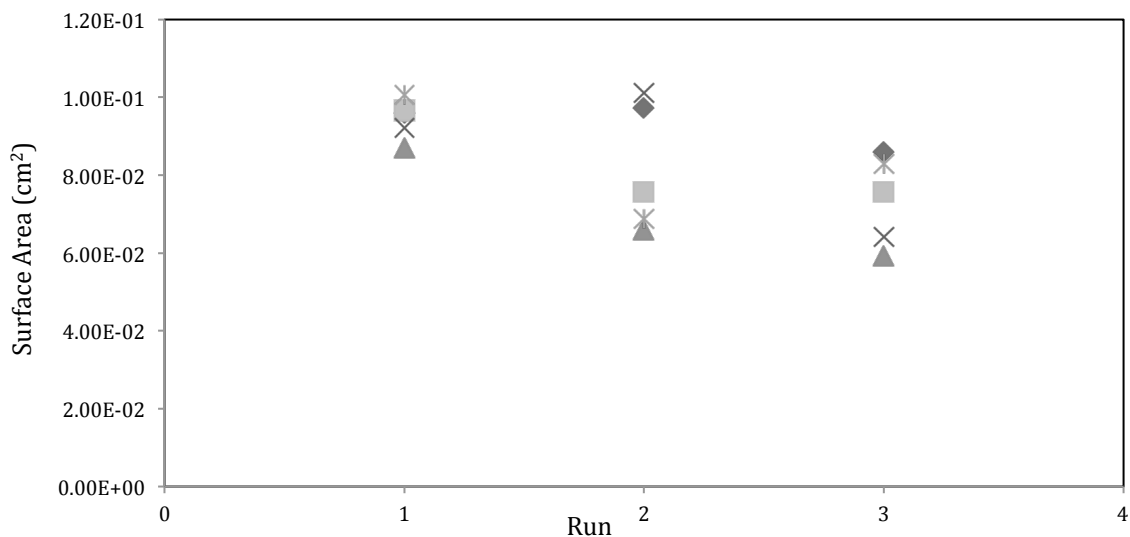


Figure 22. Surface area calculations of the gold working electrode using the quasi-reversible Randles-Sevčik method in $\text{Ru}(\text{NH}_3)_6^{2+/3+}$. Electrode 1 are the diamonds, Electrode 2 are the squares, Electrode 3 are the triangles, Electrode 4 are the x's and Electrode 5 are the x's with a line running through them.

As seen above, both of the methods used to calculate surface area produce discrepant results. A comparison between the two methods was conducted by plotting the surface area obtained from method 1 (modified Randles-Sevčik/ $\text{Ru}(\text{NH}_3)_6^{2+/3+}$) and method 2 (C_{dl} /blank buffer). By evaluating the resultant linear regression slope and y-intercept against the expected slope of 1 and y-intercept of 0, these methods can be compared.

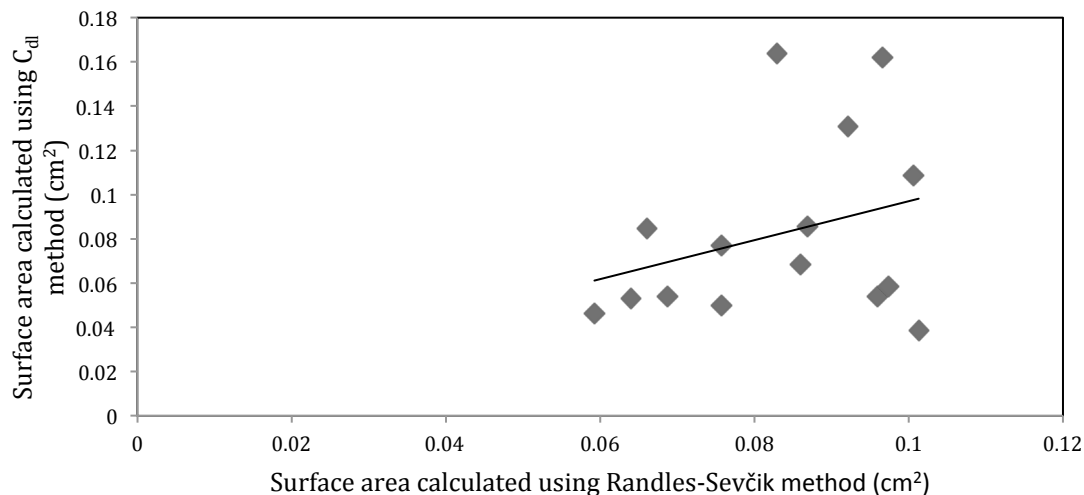


Figure 23. The comparison of both of the calculation methods for real surface area.

A linear regression was performed on the data. The slope of the line was 0.89 while the y-intercept was 0.01. The r^2 value was calculated to be 0.093. Ideally, these two methods would give the same results, resulting in a line with a slope equal to 1 and a y-intercept equal to 0. According to the data this was not the case. The slope of the ideal line, i.e., slope=1, was within the 95% confidence interval calculated during the regression, suggesting no bias. However, the low r^2 value suggests that, although producing unbiased results, the surface area calculated by the two methods have a low correlation. Also, when comparing the data obtained from the two methods, the Randles-Sevcik method produced less varied results, with a standard deviation of 0.01 than the double-layer capacitance method, with a standard deviation of 0.04, suggesting that although both methods produce similar results, the Randles-Sevcik method, experimentally, is a good method to use when attempting to determine the active surface area of an electrode.

All the estimates of real surface area are greater than the nominal surface area of 0.0314 cm². This would suggest that there is a significant amount of surface roughness. This finding is consistent with that of Churinsky, who showed that the real surface area of activated carbon electrodes are larger than the nominal surface area after sufficient activation [49].

The smallest surface area calculated for the gold screen-printed electrodes was 0.039 cm², which is greater than the nominal surface area. This is different from calculations done by others who have obtained effective surface area-to-nominal area ratios between 39% and 79%. These ratios were done on different screen-printed electrodes using the Randle-Sevčik equation [19]. The data shown here have at least a 200% surface area-to-nominal area ratio. Wan et al. conducted a study to observe the effects of activation on the performance of gold screen-printed electrodes [62]. Through the use of scanning electron microscopy, Wan observed that the surface of the electrode was rough due to formation of nanoparticle clusters on the surface of the electrodes, resulting in an increase in the active surface area [62]. This is a possible reason as to why the electrodes exhibit a higher active surface area than the nominal surface area.

The effect of reusing these electrodes was also studied. This part of the experiment was done by comparing trends in the data sets to observe if reusing the electrodes has an effect on the active surface area. The marketing of the screen-printed electrodes states that the electrode cards are for short-term uses and not long-term experiments. A study done by Almeida et al. concluded that screen-

printed gold electrodes remained stable after 15 analytical runs in 25% hydroethanolic solution before a new electrode was needed [61]. The data shown in this study is in concordance, in that the electrodes are still stable after 9 total runs, though some variation was seen.

The capacitance data for this experiment is in concordance with the literature concerning screen-printed electrodes. A study conducted by Su et al. reported increases in capacitance when cycling screen-printed carbon electrodes from -0.6 V to +1.6 V which is near the potential range used in this study [14]. The capacitance values Su reported were 3.5 $\mu\text{F}/\text{cm}^2$ before cleaning and 19.5 $\mu\text{F}/\text{cm}^2$ after cleaning [14]. The values obtained in this study ranged from 21-33 $\mu\text{F}/\text{cm}^2$ which are only slightly higher than the values obtained by Su. Cui et al. also observed that carbon electrodes exhibited a capacitance range of 20-70 $\mu\text{F}/\text{cm}^2$. Screen-printed gold values calculated during this experiment fall in this range of these capacitance values as well [60].

3.2.4 Creation of a DNA biosensor

The formation of the biosensor used a 200 nM solution of single-stranded DNA probes. The square wave voltammograms of the bare gold electrode, the MCH layer, and the monolayer were compared using the same parameters for all of the analyses. The three voltammograms were plotted on the same axis and compared (Figure 25); when analyzed, the bare gold analysis had significant background current as seen by the broad peak in Figure 24. After MCH was placed on the surface of the electrode, no identifiable signal was observed in the voltammogram. This is

presumably due to the MCH coating the surface of the electrode, which disallowed any charging or electron transfer processes from occurring.

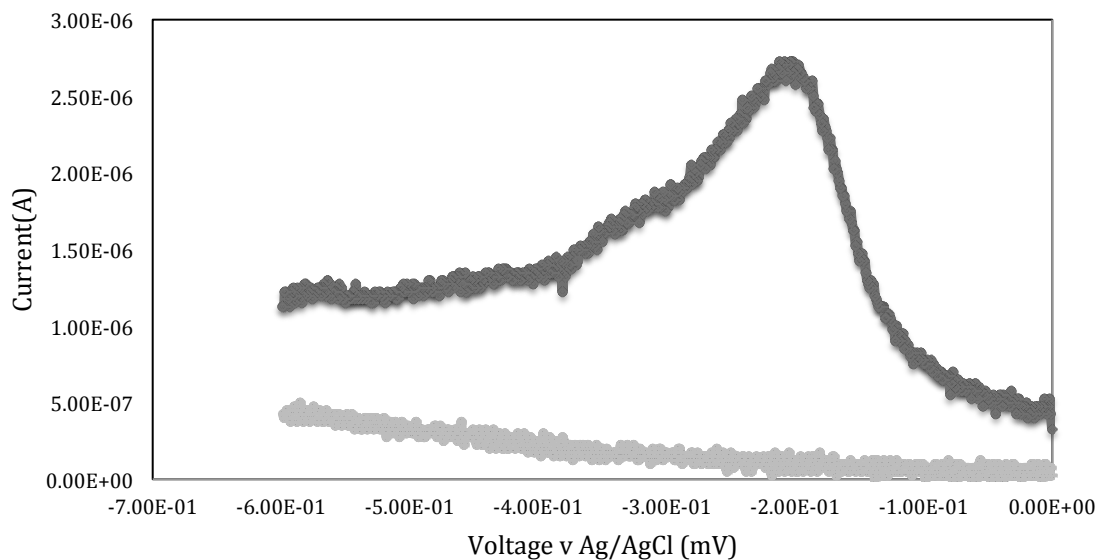


Figure 24. A SWV of the bare gold layer (dark grey) and the MCH layer (light grey).

As seen above, the MCH was successfully bound to the surface of the gold electrode due to the decrease in the signal from the bare gold to the MCH layer. The next step in creating the biosensor was to hybridize the probe DNA to the surface of the electrode. According to Rowe et al., indications of DNA chemisorption would be observed at -350 mV, which is close to the redox potential of the methylene blue redox probe [29].

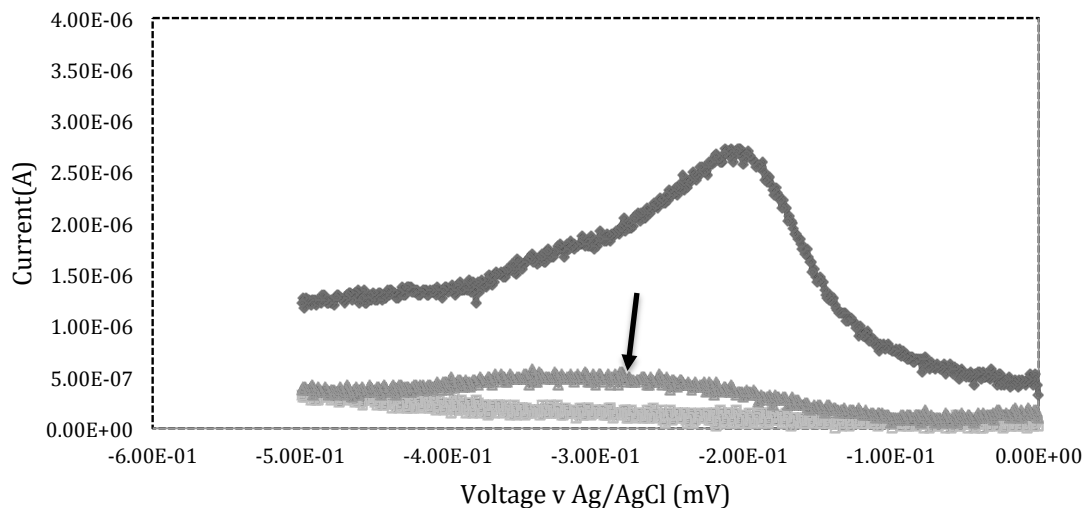


Figure 25. A SWV of the bare gold layer (dark grey), the DNA layer (the arrow pointing to the data) and the MCH layer (light grey).

Figure 25 shows the SWV when DNA was incorporated into the recognition layer and demonstrates that though a peak at approximately -350 mV is observed it is broad and weak (the dark grey with the black arrow).

3.3 Recommendation for Forensic Biosensors

This research has shown that screen-printed electrodes are not expected to exhibit a large amount of variation. They can also be reused without significant changes in active surface area. This research has also shown that MCH can adhere to the surface of the screen-printed gold electrodes in order to form a recognition layer, however, more testing needs to be performed in order to ensure that a full recognition layer which exhibits high sensitivity and selectivity can be assembled. Gold SPE's can be a good platform for a biosensor but these electrodes need more testing before it can be determined if they are reliable enough for forensic testing.

4.0 Conclusion

This work aimed to examine the surface characteristics of gold screen-printed electrodes by conducting a set of preliminary experiments to determine if a DNA recognition layer can be formed on the surface of these electrodes. The gold electrodes were observed to be reproducible and stable using both CV and SWV.

Screen-printed electrodes are useful for short experiments that are not complex. They can be used in succession without the introduction of a significant amount of signal variation. The formation of a biosensor involves different steps and more complex measurements that introduce changes to the electrode surface. Further testing needs to be performed to ensure that the DNA recognition layer can consistently be formed using these electrodes.

Quantification of forensic samples involves samples with a low concentration of DNA, so the assay that is used must be sensitive to small concentration changes. The qPCR method is sensitive enough for forensic samples but requires fluorophores and detectors to record these signals. A biosensor can provide an alternative to qPCR that is sensitive, cost effective, and time-efficient. These would be desirable characteristics for a DNA detector at a crime scene or other forensic setting. Gold screen-printed electrodes are a good choice to create the biosensor; however, optimization of the development of the recognition layer is required.

5.0 Future Research

Screen-printed gold electrodes should not be discounted for use in forensic DNA analysis without more testing and optimization. The MCH incubation step and

the DNA incubation step can be further optimized for the screen-printed gold electrode. A study conducted by Rowan stated that one hour was the optimal incubation time for DNA on gold disc electrodes [57]. This may not be the case for screen-printed gold, but more testing can be done to optimize the procedure [57]. Wan et al. also suggested that activation can lead to higher sensitivity, linearity, and lower limits of detection when determining the concentration of lead and copper in a solution [62]. Activation was not part of this study but can be tested as a possible aid to this experiment. Moreno et al. and Kuralay et al. have both shown that monolayers can be formed on the surface of screen-printed gold electrodes [63][64][65]. In conclusion, disposable, reusable, and stable SPEs have the potential to analyze not only the quantity but the quality of DNA at a crime scene. If successful, these methods can be useful to crime scene responders and forensic analysts when choosing downstream analytical processes.

REFERENCES

- [1] Jeffreys AJ, Wilson V, Thein SW. Hypervariable 'minisatellite' regions in human DNA. *Nature* 1984;314:67-73.
- [2] Giardina E, Spinella A, Novelli G. Past, present and future of forensic DNA typing. *Nanomedicine* 2011 Feb;6(2):257-270.
- [3] Jobling MA, Gill P. Encoded Evidence: DNA in Forensic Analysis. *Nature Reviews Genetics* 2004 Oct;5(10):739-751.
- [4] Saiki RK, Scharf S, Faloona F, Mullis KB, Horn TG, Erlich HA, Arnheim N. Enzymatic Amplification of β -Globin Genomic Sequences and Restriction Site Analysis for Diagnosis of Sickle Cell Anemia. *Science* 1985 Dec;230(4732):1350-1354.
- [5] Budowle B, Moretti TR, Baumstark AL, Defenbaugh DA, Keys KM. Population Data on the Thirteen CODIS Core Short Tandem Repeat Loci in African Americans, U.S. Caucasians, Hispanics, Bahamians, Jamaicans, and Trinidadians. *Journal of Forensic Sciences* 1999 Nov;44(6):1277-1286.
- [6] Butler JM. *Fundamentals of Forensic DNA Typing*. Burlington: Academic Press, 2010.
- [7] Kerman K, Vestergaard M, Tamiya E. Electrochemical DNA Biosensors: Protocols for Intercalator-Based Detection of Hybridization in Solution and at the Surface. In: Rasooly A, Herold KE, editors. *Methods in Molecular Biology: Biosensors and Biodetection*, Vol. 504. New York: Humana Press, 2009;99-113.
- [8] Lucarelli F, Marrazza G, Turner APF, Mascini M. Carbon and gold electrodes as electrochemical transducers for DNA hybridisation sensors. *Biosensors and Bioelectronics* 2004;19:515-530.
- [9] Life Technologies Corporation. *Applied Biosystems Quantifiler® Duo DNA Quantification Kit User's Manual*. Grand Island: Life Technologies Corporation, 2012.
- [10] Horsman KM, Hickey JA, Cotton RW, Landers JP, Maddox LO. Development of a Human-Specific Real-Time PCR Assay for the Simultaneous Quantitation of Total Genomic and Male DNA. *Journal of Forensic Sciences* 2006 Jul;51(4):758-765.

- [11] Kazuo Nakazato (2013). Potentiometric, Amperometric, and Impedimetric CMOS Biosensor Array, State of the Art in Biosensors - General Aspects, Dr. Toonika Rinken (Ed.), ISBN: 978-953-51-1004-0, InTech, DOI: 10.5772/53319. Available from: <http://www.intechopen.com/books/state-of-the-art-in-biosensors-general-aspects/potentiometric-amperometric-and-impedimetric-cmos-biosensor-array>.
- [12] McConaughy BL, Laird CD, McCarthy BJ. Nucleic Acid Reassociation in Formamide. *Biochemistry* 1969 Aug;8(8):3289-3295.
- [13] Pine Research Instrumentation. Working with Pine Screen Printed Electrodes. REV 007 (Jul 2008).
- [14] Su WY, Wang SM, Cheng SH. Electrochemically pretreated screen- printed carbon electrodes for the simultaneous determination of aminophenol isomers. *Journal of Electroanalytical Chemistry* 2011;651:166-172.
- [15] Yang TH, Hung CL, Ke JH, Zen JM. An electrochemically preanodized screen-printed carbon electrode for achieving direct electron transfer to glucose oxidase. *Electrochemistry Communications* 2008;10:1094-1097.
- [16] Prasad KS, Muthuraman G, Zen JM. The role of oxygen functionalities and edge plane sites on screen-printed carbon electrodes for simultaneous determination of dopamine, uric acid and ascorbic acid. *Electrochemistry Communications* 2008;10:559-563.
- [17] Herne TM, Tarlov MJ. Characterization of DNA Probes Immobilized on Gold Surfaces. *Journal of the American Chemical Society* 1997;119:8916-8920.
- [18] Pine Research Instrumentation. Working with Pine Ceramic Patterned Electrodes. REV 007 (Jul 2008).
- [19] Kadara RO, Jenkinson N, Banks CE. Characterisation of commercially available electrochemical sensing platforms. *Sensors and Actuators B: Chemical* 2009;138:556-562.
- [20] Fanjul-Bolado P, Hernández-Santos D, Lamas-Ardisana PJ, Martín-Pernía A, Costa-García A. Electrochemical characterization of screen-printed and conventional carbon paste electrodes. *Electrochimica Acta* 2008;53:3635-3642.
- [21] Vanysek P, Gauthier P. Disposable Graphite Electrode for Studies of Catalytic Layers of Platinum. *Journal of New Materials for Electrochemical Systems* 2008;11:157-163.

- [22] Gileadi E. *Electrode Kinetics for Chemists, Chemical Engineers, and Materials Scientists*. New York: Wiley-VCH, Inc., 1993.
- [23] “Ru Estimation,” “Purpose” help file [Echem Analyst™, version 5.60]. MS Windows 7. Warminster (PA): Gamry, 2011.
- [24] Gornall DD, Collyer SD, Higson SPJ. Investigations into the use of screen-printed carbon electrodes as templates for electrochemical sensors and sonochemically fabricated microelectrode arrays. *Sensors and Actuators B: Chemical* 2009;141:581-591.
- [25] Labuda J, Brett AMO, Evtugyn G, Fojta M, Mascini M, Ozsoz M, Palchetti, Paleček E, Wang J. *Electrochemical nucleic acid-based biosensors: Concepts, terms and methodology (IUPAC Technical Report)*. *Pure and Applied Chemistry* 2010 Apr;82(5):1161-1187.
- [26] Gonçalves LM, Batchelor-McAuley C, Xiong L, Barros AA, Compton RG. The Voltammetric Responses of High and Low Molecular Weight DNA on a Variety of Carbon Substrates; Demonstrating the Benefits of Graphitic Surfaces. *Electroanalysis* 2011;23(3):583-587.
- [27] Wang J, Cai X, Tian B, Shiraishi H. Microfabricated Thick-film Electrochemical Sensor for Nucleic Acid Determination. *Analyst* 1996 Jul;121:965-970.
- [28] Wang J, Rivas G, Fernandes JR, Paz JLL, Jiang M, Waymire R. Indicator-free electrochemical DNA hybridization sensor. *Analytica Chimica Acta* 1998;375:197-203.
- [29] Rowe AA, White RJ, Bonham AJ, Plaxco KW. *Fabrication of Electrochemical-DNA Biosensors for the Reagentless Detection of Nucleic Acids, Proteins and Small Molecules.pdf*. *J Vis Exp [Internet]* 2011. Available from: <http://www.jove.com/video/2922>.
- [30] Osteryoung JG, Osteryoung RA. Square wave voltammetry. *Anal Chem* 1985;57(1):101A-110A.
- [31] “Understanding the Different Methods to Electrochemical Analysis.” <http://www.azom.com/article.aspx?ArticleID=10624>. 2014 Feb 6.
- [32] Gill P, Curran J, Elliot K. A graphical simulation model of the entire DNA process associated with the analysis of short tandem repeat loci. *Nucleic Acids Research* 2005;33(2):632-643.
- [33] Pine Instrument Company. *Educator’s Reference Guide for Electrochemistry, Manual LMPROF1 Revision 003 Feb 2000*.

- [34] “EXPERIMENT 5. CYCLIC VOLTAMMETRY.” <http://www2.chemistry.msu.edu/courses/cem419/cem372cyclicvoltammetry.pdf>.
- [35] Kissinger PT, Heineman WR. Cyclic Voltammetry. *Journal of Chemical Education* 1983 Sept;60(9):702-706.
- [36] Wang J. *Analytical Electrochemistry*. 3rd ed. Hoboken: John Wiley & Sons, 2006.
- [37] Grgicak CM. Alternative anode materials for solid oxide fuel cell (SOFC) systems operating in multiple fuel environments [dissertation]. Ottawa, (ON): University of Ottawa, 2007.
- [38] Kounaves SP. Voltammetric techniques. *Handbook of Instrumental Techniques for Analytical Chemistry* 1997;709–26.
- [39] Princeton Applied Research. Application Note S-7: Square Wave Voltammetry. 1984.
- [40] Ramaley L, Krause Jr MS. Theory of square wave voltammetry. *Anal Chem* 1969;41(11):1362–5.
- [41] Timken MD, Swango KL, Orrego C, Chong MD, Buoncristiani MR. Quantitation of DNA for Forensic DNA Typing by qPCR (quantitative PCR): Singleplex and Multiplex Modes for Nuclear and Mitochondrial Genomes, and the Y Chromosome. Richmond (CA): California Department of Justice, Jan Bashinski DNA Laboratory; 2005 Jun. Report No.:210302 (NIJ Award No. 2002-IJ-CX-K008).
- [42] Nolan T, Hands RE, Bustin SA. Quantification of mRNA using real-time RT-PCR. *Nature Protocols* 2006 Nov;1(3):1559-1582.
- [43] Smith CJ, Osborn AM. Advantages and limitations of quantitative PCR (Q-PCR)-based approaches in microbial ecology. *FEMS Microbiology Ecology* 2009;67(1):6-20.
- [44] Grgicak CM, Urban ZM, Cotton RW. Investigation of Reproducibility and Error Associated with qPCR Methods using Quantifiler® Duo DNA Quantification Kit. *Journal of Forensic Sciences* 2010;55(5):1331-1339.
- [45] Wang J. Electrochemical nucleic acid biosensors. *Analytica Chimica Acta* 2002;469:63-71.
- [46] Steichen M, Buess-Herman C. Electrochemical detection of the immobilization and hybridization of unlabeled linear and hairpin DNA on gold. *Electrochemistry Communications* 2005;7:416-420.

- [47] Square Wave Voltammogram <http://www.electronics-tutorials.ws/waveforms/waveforms.html>.
- [48] Wang J, Pedrero M, Sakslund H, Hammerich O, Pingarron J. Electrochemical Activation of Screen-Printed Carbon Strips. *Analyst* 1996 Mar;121:345-350.
- [49] Churinsky, Candace. Characterization of Carbon Electrode Surfaces: Development of Biosensors for Forensic DNA Applications. Boston University Biomedical Forensic Sciences Master's Thesis. 2013.
- [50] BioLogic Science Instruments. Application note #21: Measurements of the double layer capacitance. "<http://www.bio-logic.info/potentiostat/notes/20101209%20%20Application%20note%2021.pdf>."
- [51] Weingärtner H. The Static Dielectric Constant of Ionic Liquids. *Zeitschrift für Physikalische Chemie* 2006;220:1395-1405.
- [52] "Propagation of uncertainty," http://en.wikipedia.org/wiki/Propagation_of_uncertainty.
- [53] "Error Propagation," <http://mathworld.wolfram.com/ErrorPropagation.html>.
- [54] Grgicak, CM. Notes from Adv. Topics in Forensic Chemistry. Boston University Biomedical Forensic Sciences Masters Course. Summer 2014.
- [55] Wang Y, Limon-Petersen JG, Compton RG. Measurement of the diffusion coefficients of $[\text{Ru}(\text{NH}_3)_6]^{3+}$ and $[\text{Ru}(\text{NH}_3)_6]^{2+}$ in aqueous solution using microelectrode double potential step chronoamperometry. *Journal of Analytical Chemistry* 2011;652:13-17.
- [56] Ganesh V, Pal SK, Kumar S, Lakshminarayanan V. Self-assembled monolayers (SAMs) of alkoxy cyanobiphenyl thiols on gold—A study of electron transfer reaction using cyclic voltammetry and electrochemical impedance spectroscopy. *J Colloid Interface Sci* 2006;296(1):195–203.
- [57] Rowan, Kayleigh. Characterizing Variability in Fluorescence-Based Forensic DNA Measurement and Developing an Electrochemical-Based Quantification System. Boston University Biomedical Forensic Sciences Master's Thesis. 2014.
- [58] Sánchez-Pomales G, Santiago-Rodríguez L, Rivera-Vélez NE, Cabrera CR. Control of DNA self-assembled monolayers surface coverage by electrochemical desorption. *J Electroanal Chem* 2007;611(1-2):80–6.
- [59] Herskovits TT. Nonaqueous Solutions of DNA; Denaturation by Urea and Its Methyl Derivatives. *Biochemistry* 1963 Mar;2(2):335-340.

- [60] Cui G, Yoo JH, Lee JS, Yoo J, Uhm JH, Cha GS, Nam H. Effect of pretreatment on the surface and electrochemical properties of screen-printed carbon paste electrodes. *The Analyst* 2001;126:1399-1403.
- [61] Almeida E, Richter E, Muzoz R. On-site fuel electroanalysis: Determination of lead, copper and mercury in fuel bioethanol by anodic stripping voltammetry using screen-printed gold electrodes. *Analytica Chimica Acta* 837 (2014);38-43.
- [62] Wan H, Sun Q, Li H, Sun F, Hu N, Wang P. Screen-printed gold electrode with gold nanoparticles modification for simultaneous electrochemical determination of lead and copper. *Sensors and Actuators B: Chemical* 209 (2015); 336-342.
- [63] Moreno M, Rincon E, Pérez J. Selective immobilization of oligonucleotide-modified gold nanoparticles by electrodeposition on screen-printed electrodes. *Biosens Bioelectron* (2009) 25:778–783.
- [64] Kuralay F, Campuzano S, Haake DA, Wang J. Highly sensitive disposable nucleic acid biosensors for direct bioelectronic detection in raw biological samples. *Talanta* (2011) 85:1330–1337.
- [65] Taleat Z, Khoshroo A, Mazloum-Ardakani M. Screen-printed electrodes for biosensing: a review (2008-2013). *Microchim Acta* (2014) 181:865-891.
- [66] Levicky R, Herne TM, Tarlov MJ, Satija SK. Using Self-Assembly To Control the Structure of DNA Monolayers on Gold: A Neutron Reflectivity Study. *J Am Chem Soc* 1998;120:9787–92.

CURRICULUM VITAE

